Asymmetric requirement of Dpp/BMP morphogen dispersal in the Drosophila wing disc

Shinya Matsuda[*1], Jonas V. Schaefer[2], Yusuke Mii[3], Yutaro Hori[4], Dimitri Bieli[1], Masanori Taira[5], Andreas Plückthun[2], and Markus Affolter[*1]

Affiliations:

1. Biozentrum, University of Basel, Switzerland
2. Department of Biochemistry, University of Zurich, Switzerland
3. National Institute for Basic Biology and Exploratory Research Center on Life and Living Systems (ExCELLS), National Institutes of Natural Sciences, Japan
   JST, PRESTO, Japan
4. Institute for Quantitative Biosciences, The University of Tokyo, Japan
5. Department of Biological Sciences, Graduate School of Science, The University of Tokyo, Japan
   Present address: Department of Biological Sciences, Faculty of Science and Engineering, Chuo University, Japan

Corresponding authors

Correspondence to: markus.affolter@unibas.ch or shinya.matsuda@unibas.ch

Summary

Morphogen gradients provide positional information and control growth in developing tissues, but the underlying mechanisms remain largely unknown due to lack of tools manipulating morphogen gradients. Here, we generate two synthetic protein binder tools manipulating different parameters of Decapentaplegic (Dpp), a morphogen thought to control Drosophila wing disc patterning and growth by dispersal; while HA trap blocks Dpp dispersal, Dpp trap blocks Dpp dispersal and signaling in the source cells. Using these tools, we found that while posterior patterning and growth require Dpp dispersal, anterior patterning and growth largely proceed without Dpp dispersal. We show that *dpp* transcriptional refinement from an initially uniform to a localized expression and persistent signaling in transient *dpp* source cells render the anterior compartment robust to blocking Dpp dispersal. Furthermore, neither Dpp dispersal nor signaling is critical for lateral wing growth. These results challenge Dpp dispersal-centric mechanisms, and demonstrate the utility of customized protein binder tools to dissect protein functions.

Introduction

A fundamental question in developmental biology is how proteins work together to orchestrate developmental processes. Forward and reverse genetic approaches based on mutants and RNAi, together with biochemical analyses, provide insights into how proteins function. However, interpretational gaps often remain between the mutant phenotypes and the underlying mechanisms.

Recently, small, high affinity protein binders such as nanobodies, single-chain variable fragment (scFv), Designed Ankyrin Repeat Proteins (DARPins) and others have emerged as versatile tools to fill this gap. By fusing these protein binders to well-characterized protein domains and expressing the fusion proteins *in vivo*, protein function can be directly manipulated in a predicted manner [1-4]. For example, to characterize a protein with multiple functions, these tools could allow to manipulate a given function without affecting others, thereby allowing a better dissection of each function. To investigate a protein function consisting of multiple parameters, applying different protein binder tools targeting each or a subset of parameters and comparing the effects with mutants could help to better dissect how a protein exerts its function. However, it remains challenging to design and customize distinct protein binder tools targeting different parameters to investigate protein functions consisting of multiple parameters.

A class of molecules that exert its function with multiple parameters are morphogens, secreted molecules that disperse from a localized source and regulate target gene expression in a concentration-dependent manner [5-8]. A morphogen gradient is characterized by its parameters such as secretion, diffusion, and degradation [9]. Temporal dynamics of a morphogen gradient also impact cell fates decisions [10]. Despite a variety of parameters involved, morphogen dispersal is generally thought to be critical for a morphogen function based on severe morphogen mutant phenotypes and long-range action of morphogens.

However, a recent study challenged this basic assumption for the case of the Wingless (Wg) morphogen, the main Wnt in Drosophila, by showing that a membrane-tethered non-diffusible form of Wg can replace the endogenous Wg without affecting appendages development [11]. Although the precise contribution of Wg dispersal requires further studies [12-15], the study raises the question of how important morphogen dispersal is for tissue patterning and growth in general.

In contrast to Wg, *Decapentaplegic (dpp)*, the vertebrate BMP2/4 homologue, is thought to act as a *bona fide* morphogen in the Drosophila prospective wing. Dpp disperses bidirectionally from a narrow anterior stripe of cells along the anterior-posterior (A-P) compartment boundary to establish a characteristic morphogen gradient in both compartments [16, 17]. How the Dpp dispersal-mediated morphogen gradient achieves and coordinates overall wing patterning and growth has served as a paradigm to study morphogens [18]. However, despite intensive studies, it remains controversial how Dpp/BMP disperses [16, 19-22], controls uniform growth [23-29], and coordinates patterning and growth (i.e. scaling) [30-33]. Regardless of the actual mechanisms, all the studies are based on the assumption that bidirectional Dpp dispersal from the anterior stripe of cells controls overall wing patterning and growth, in line with the severe *dpp* mutant phenotypes.

To directly manipulate dispersal of Dpp, we recently generated a synthetic protein binder tool called morphotrap, a membrane-tethered anti-GFP nanobody, to trap GFP-tagged Dpp and thereby manipulating its dispersal [34]. Using morphotrap, we showed that a substantial amount of GFP-Dpp secreted from the anterior stripe of cells can reach to the peripheral wing disc and blocking GFP-Dpp dispersal from the source cells cause severe adult wing patterning and growth defects [34]. These results support the assumption that Dpp dispersal from the anterior stripe of cells is critical for overall wing patterning and growth (Fig. 1a) [34]. However, application of morphotrap was limited to rescue conditions by overexpression of GFP-Dpp due to the lack of an endogenous *GFP-dpp* allele.

Here, to investigate the precise requirement of endogenous Dpp morphogen gradient for wing patterning and growth, we first generated an endogenous *GFP-dpp* allele, but found that the allele was not fully functional, thus limiting morphotrap application. We then generated two synthetic protein binder tools analogous to morphotrap, manipulating distinct aspects of endogenous Dpp morphogen

gradient; while "HA trap" blocks functional Dpp dispersal, "Dpp trap" blocks Dpp dispersal and signaling in the source cells. Using these tools, we found that while Dpp signaling in the source cells is critical, the role of Dpp dispersal is surprisingly minor and asymmetric for wing patterning and growth; while posterior patterning and growth require Dpp dispersal, anterior patterning and growth largely proceed without Dpp dispersal. We show that previously unrecognized *dpp* transcriptional refinement from an initially uniform to a localized expression and persistent signaling in transient *dpp* source cells allow the anterior patterning and growth robust to blocking Dpp dispersal. Furthermore, we find that neither Dpp dispersal nor signaling is critical for the lateral wing pouch growth. These results challenge the long-standing dogma that Dpp dispersal is essential to control overall wing patterning and growth and call for a revision of how Dpp controls and coordinates wing patterning and growth.

Results

A platform to manipulate the endogenous *dpp* locus

To manipulate the endogenous Dpp morphogen gradient, we utilized a MiMIC transposon inserted in the *dpp* locus [35]. A genomic fragment containing sequences encoding a tagged version of *dpp* followed by an FRT and a marker was first inserted into the locus (Fig. 1b), then the endogenous *dpp* exon was removed upon FLP/FRT recombination to keep only the tagged *dpp* exon (Fig. 1b). Using this strategy, we inserted different tags into the *dpp* locus and found that while a *GFP-dpp* allele was homozygous lethal during early embryogenesis (data not shown), a *HA-dpp* allele was functional without obvious phenotypes (Fig. 1c). A similar functional HA tag knock-in *dpp* allele has recently been generated by a CRISPR approach [29]. HA-Dpp was expressed in the anterior stripe of cells along the A-P compartment boundary consistent with reported *dpp* expression pattern (Fig. 1d) and the extracellular HA-Dpp gradient overlapped with the gradient of phosphorylated Mad (pMad), a downstream transcription factor of Dpp signaling (Fig. 1e).

Generation and characterization of HA trap

Since we could not apply morphotrap due to the lethality of the *GFP-dpp* allele, we generated a protein binder tool called "HA trap" by fusing an anti-HA scFv to the transmembrane domain of CD8 and mCherry, analogous to morphotrap (Fig. 1f). To visualize Dpp upon trapping, we also generated a functional *Ollas-HA-dpp* allele. Upon HA trap expression using *ptc-Gal4* in an *Ollas-HA-dpp/+* wing disc, Ollas-HA-Dpp accumulated on the anterior stripe of cells, and the extracellular gradient was abolished (Fig. 1g-j). Furthermore, clonal accumulation of Ollas-HA-Dpp in HA trap clones in the receiving cells was undetectable upon HA trap expression with *ptc-Gal4* (Fig. 1k-n, arrow), indicating that the HA trap can block HA-Dpp dispersal efficiently like morphotrap. However, in contrast to morphotrap, Ollas-HA-Dpp accumulated in HA trap clones near the source but not in the peripheral regions (Fig. 1o arrowhead), raising the question whether Dpp can act in the peripheral regions.

Blocking Dpp dispersal by HA trap causes minor and asymmetric patterning and growth defects

To address the requirement of Dpp dispersal, we expressed HA trap using different *Gal4* driver lines in *HA-dpp* homozygous wing discs. Normally, Dpp binds to the Dpp receptors Thickveins (Tkv) and Punt, inducing a pMad gradient and an inverse gradient of Brk, a transcription repressor repressed by Dpp signaling. The two opposite gradients regulate patterning (nested target gene expression, such as *sal*, and *omb*) and growth to define adult wing vein positions and control growth [18, 36-39] (Fig. 2a). Upon HA trap expression using *ptc-Gal4*, pMad, Sal, and Omb expression were completely lost and Brk was upregulated in the P compartment (Fig. 2b, e, f, g, h), indicating that HA trap efficiently blocked HA-Dpp dispersal. Interestingly, despite undetectable Dpp signaling, the posterior wing pouch grew substantially as judged by the expression of an intervein marker DSRF and a wing pouch marker *5xQE.DsRed* (a reporter of the Quadrant Enhancer (QE) of the wing master gene *vg*) (Fig. 2b arrow, 2i). In the A compartment, pMad was slightly reduced in the anterior medial region (Fig. 2b, e),

probably because HA trap partially blocked Dpp signaling upon binding to HA-Dpp (Fig. 1n). Nevertheless, anterior patterning (nested expression of Sal and Omb) and growth were relatively normal (Fig. 2b). Consequently, the resulting adult wings showed relatively mild anterior and severe posterior patterning and growth defects with substantial posterior lateral growth (Fig. 2c, d). Slightly milder but similar phenotypes were observed upon HA trap expression using *nub-Gal4* (Fig. 2k-t) and *ci-Gal4* (Extended Data Fig. 2a-j). The severe posterior growth defects were not due to cell death, since Caspase-3 was not upregulated (Extended Data Fig. 1a, b, d), and blocking apoptosis by apoptosis inhibitor p35 did not rescue these growth defects (Extended Data Fig. 1e-g). These results suggest that, while critical for posterior patterning and growth, Dpp dispersal is largely dispensable for anterior patterning and growth, and that posterior lateral region can grow without Dpp dispersal and signaling.

Lateral wing pouch growth without Dpp signaling

Since Dpp dispersal- and signaling-independent posterior wing pouch growth contradicts previous reports [40, 41], we tested whether there was a substantial leakage of Dpp from the HA trap. When tkv^{a12} clones characterized as a null allele [42, 43] were induced in wing discs expressing HA trap with *ptc-Gal4*, tkv^{a12} clones survived and expressed the *5xQE.DsRed* reporter in the anterior lateral regions as well as in the entire posterior region, even next to the source cells (Fig. 3a), indicating that leakage is negligible. Similarly, tkv^{a12} clones induced in the wild type wing disc survived and expressed the *5xQE.DsRed* reporter in the lateral wing pouch (Fig. 3b). We also generated a *tkv* flip-out allele by inserting an FRT cassette in the *tkv* locus ($tkvHA^{FO}$) and confirmed these results (Fig. 3c, d arrow). In rare cases, even medial *tkv* null clones survived and expressed *5xQE.DsRed* (Fig. 3d), indicating that the elimination of *tkv* mutant clones masked Dpp signaling-independent *5xQE.DsRed* expression in previous studies. Consistently, upon genetic removal of *dpp* from the entire A compartment as early as the beginning of second instar stage, when the wing pouch is defined, *5xQE.DsRed* remained expressed despite severe growth defects (Fig. 3e-h). Furthermore, the loss of *5xQE.DsRed* reporter expression in *dpp* mutants was rescued in *dpp, brk* double mutant wing discs (Extended Data Fig. 3). Taken together, these results indicate that lateral wing pouch can grow without direct Dpp signaling input after wing pouch specification.

Blocking Dpp dispersal and signaling by Dpp trap causes severe defects similar to *dpp* mutant

How can relatively normal patterning and growth be achieved without Dpp dispersal? Given the substantial pMad signal in the source cells upon HA trap expression (Fig. 2b, l), we hypothesized that Dpp signaling in the source cells could account for the minor phenotypes caused by HA trap. To test this, we avoided genetic removal of *tkv* since *tkv* affects Dpp dispersal non-autonomously [44, 45]. Instead, we selected DARPins [46] against purified Dpp. For each of the 36 candidates from the screening, we generated a "Dpp trap" by fusing the anti-Dpp DARPin to the transmembrane domain of CD8 and mCherry (Fig. 4a), and identified one Dpp trap (containing DARPin 1242_F1), which efficiently blocked Dpp dispersal and signaling (Fig. 4b, 4d, 4l, Extended Data Fig. 2k). We found that Dpp trap caused more severe defects than HA trap using *ptc-Gal4* (Fig. 4d, 2b), *nub-Gal4* (Fig. 4l, 4n, 2l, 2n), and *ci-Gal4* (Extended Data Fig. 2). Adult wings expressing Dpp trap using *nub-Gal4* were recovered and phenocopied severe *dpp* mutants (Fig. 4n, 3g, 3h). Interestingly, anterior Dpp trap expression caused more severe posterior growth defects as well as anterior growth defects than HA trap (Fig. 4j, Extended Data Fig. 2u). This non-autonomous effect was hardly seen by simply removing *tkv* from the entire A compartment, probably because Dpp can still disperse and control patterning and growth under this condition (data not shown). Since HA trap blocks Dpp dispersal more efficiently than Dpp trap (Extended Data Fig. 4), these severe phenotypes by Dpp trap is rather due to blocking Dpp signaling by Dpp trap. Although Caspase-3 was upregulated upon Dpp trap expression with *nub-Gal4* (Extended Data Fig. 1a, c, d), the growth defects were not rescued by p35 (Extended Data Fig. 1h-j), indicating that apoptosis was not the main cause of growth defects by Dpp trap. Taken together, these

results suggest that Dpp signaling in the source cells is required for anterior patterning and growth as well as for posterior growth seen upon blocking Dpp dispersal by HA trap.

Rescue of *dpp* mutant by cell-autonomous Dpp signaling mimics phenotypes caused by HA trap

To test whether cell-autonomous Dpp signaling is sufficient to control patterning and growth, a constitutively active version of Tkv (TkvQD) [43] was expressed in *dpp* mutants with *dpp-Gal4* (Fig. 5a, b). We found that, despite localized pMad activation in the anterior stripe of cells, anterior patterning and growth as well as part of posterior growth were largely restored, mimicking the phenotypes caused by HA trap (Fig. 2b, 5b). These results indicate that the phenotypes caused by HA trap largely depends on Dpp signaling in the source cells. How can local Dpp signaling in the source cells control patterning and growth extending beyond the anterior stripe of cells? First, we asked how anterior Dpp signaling can control posterior growth. One trivial possibility is that the posterior growth was induced by non-specific *dpp-Gal4* expression in the P compartment. To test this, *dpp-Gal4* was converted into a ubiquitous *LexA* driver, which was permanently expressed in lineages of *dpp-Gal4* to express TkvQD (Fig. 5c). We found that although pMad was upregulated only in the A compartment (Fig. 5d), *5xQE.DsRed* expression was induced in the P compartment (Fig. 5d arrow), indicating that non-autonomous posterior growth control by anterior Dpp signaling is permissive rather than instructive.

Initial uniform *dpp* transcription in the anterior compartment

Next, we asked how Dpp signaling in the source cells can control anterior patterning and growth (Fig. 1d). It has been shown that the lineages of *dpp-Gal4* was uniform in the A compartment [47]. Consistently, the lineages of *dpp-Gal4* indicated by pMad signal was also uniform in the A compartment (Fig. 5d), raising the possibility that *dpp* expression is uniform in the early stages. Since the existing *dpp-Gal4* line is derived from a fragment of the *dpp* disc enhancer inserted outside the *dpp* locus, we first generated an endogenous *dpp-Gal4* line using our platform (Fig. 6a), and confirmed the uniform anterior lineages with G-TRACE analysis (Fig. 6b). To directly follow *dpp* transcription, we then generated a *dpp* transcription reporter line by inserting a destabilized GFP (half-life <2 hrs) into the *dpp* locus (Fig. 6c), and indeed found initial uniform anterior *dpp* transcription until the early third instar stage (Fig. 6d, e) prior to a narrow anterior stripe expression from the mid-third instar stage onwards (Fig. 6f, g).

Transient *dpp* source outside Sal domain is required for anterior patterning and growth

The earlier anterior *dpp* source outside the stripe of cells could provide a local *dpp* source to control anterior patterning and growth when Dpp dispersal is blocked. However, in such a scenario, since *ptc-Gal4* is also initially expressed in the entire A compartment [48], the minor defects by HA trap could be explained by the perdurance of Dpp signaling via artificially stabilized Dpp by HA trap. To avoid such potential artificial effects, we expressed HA trap with *ptc*-Gal4 at defined time points using *tubGal80ts*. Upon HA trap expression from the mid-second instar stage, the lineage of *ptc-Gal4* covered at most the anterior Sal domain, which corresponds to the region between L2 and L4 in the adult wing (Fig. 7b). Nevertheless, the anterior peripheral regions remained rather normal (Extended Data Fig. 5), consistent with a role of the *dpp* source outside the Sal domain for patterning and/or growth.

To test this, *dpp* was genetically removed using *ptc*-Gal4 approximately from the anterior Sal region, where cells in which the FRT cassette was removed were marked by lacZ staining (Fig. 7a-f). Consistent with the removal of the *dpp* stripe expression, pMad, Sal, and Omb were significantly reduced in the P compartment (Fig. 7d-f). In contrast, in the A compartment, low levels of pMad remained active and Brk was graded with lowest expression outside the Sal region (Fig. 7d). Under this condition, while Sal expression was completely lost, weak anterior Omb expression remained activated with highest signal in the lateral region (Fig. 7e, f). By removing *dpp* from the entire A compartment, this weak anterior Dpp signaling (pMad and Omb expression) as well as anterior growth

were severely affected (Fig. 7g-k), indicating that the transient *dpp* source outside the Sal domain contributes to anterior patterning and growth. Consistently, weak pMad and Omb expression remained rather normal in the anterior lateral region upon blocking Dpp dispersal by HA trap using *ptc-Gal4* (Fig. 2e, h). We then asked how the transient *dpp* source can lead to persistent Dpp signaling. Upon genetic removal of *tkv*, Brk was quickly de-repressed (Extended Data Fig. 6), indicating that the "memory" of an earlier signal is not mediated by epigenetic regulation or autoregulation of target gene expression but rather at the level of Tkv or upstream, consistent with weak but persistent pMad signal. The anterior patterning and growth can therefore be achieved without Dpp dispersal by a combination of a persistent signaling by transient *dpp* transcription outside the stripe and a stronger signaling by continuous *dpp* transcription in the anterior stripe of cells.

Discussion

Although protein binders have emerged as versatile tools to study protein functions, it remains challenging to design and customize distinct protein binder tools to dissect protein function. Here, we generate two novel protein binder tools to manipulate distinct parameters of the Dpp morphogen to precisely determine the requirement of Dpp dispersal and signaling in the source cells.

New protein binder tools manipulating distinct aspects of Dpp

Among protein binders against commonly used tags, nanobodies against GFP are used most intensively in the field [49]. However, since tagging with a large tag such as GFP could affect protein functions, as is the case for Dpp, protein binders against small tags have recently been generated to manipulate intracellular proteins [50-53]. Here, we show that HA trap works as efficient as morphotrap, providing an alternative way to trap secreted proteins via a small tag. Nevertheless, we found some differences between two traps. First, morphotrap appears leaky since trapping GFP-Dpp by morphotrap in the source activate Dpp signaling in at least one cell row in the P compartment [34]. Second, while morphotrap could accumulate GFP-Dpp even in the peripheral regions [34], HA trap did not (Fig. 1n). Third, while morphotrap caused severe adult wing defects [34], HA trap caused relatively minor defects (Fig. 2). We speculate that these differences are caused by overexpression of GFP-Dpp; persistent strong Dpp signaling could lead to cause cell death as shown previously [24, 54-56]. These differences highlight the importance of investigating endogenous protein functions.

In contrast to protein binders against commonly used tags, protein binders against endogenous proteins are rarely used due to the limited availability and difficulty in isolating them. Here, we screened DARPins against Dpp, and generated Dpp trap analogous to HA trap. Interestingly, we found that the two traps manipulate different parameters of Dpp morphogen gradient formation; while HA trap mainly blocks Dpp dispersal (Fig. 2), Dpp trap blocks Dpp dispersal and cell-autonomous signaling (Fig. 4). We speculate that HA trap binds to the HA tag, thereby allowing Dpp to bind to its receptors, while Dpp trap directly binds to Dpp to block its interaction with the receptors. Regardless of the actual mechanisms underlying this difference, these tools allow to dissect each requirement. Relatively mild phenotypes by HA trap and severe phenotypes by Dpp trap indicate a minor and asymmetric role of Dpp dispersal and a critical role of Dpp signaling in the source cells for wing patterning and growth, respectively. Furthermore, these results also suggest that, unlike previously thought, severe *dpp* mutant phenotypes do not reflect the role of Dpp dispersal alone, but reflect the role of both Dpp dispersal and signaling in the source cells, with more contribution from the latter parameter.

Asymmetric requirement of Dpp dispersal

It has long been thought that the bidirectional Dpp dispersal from the narrow anterior stripe of cells generate morphogen gradient in both compartments to control overall wing patterning and growth based on the critical requirement of *dpp* for wing development (Fig. 8a). A previous study using morphotrap also supported this view based on the severe adult wing defects upon morphotrap

expression [34]. Using HA trap and Dpp trap, we here show that the role of Dpp dispersal is surprisingly minor and asymmetric along the A-P axis; while posterior patterning and medial growth requires Dpp dispersal, anterior patterning and growth largely proceeds without Dpp dispersal (Fig. 2, 8b), although Dpp disperses bidirectionally from the anterior stripe of cells and generate a morphogen gradient in the late third instar stage (Fig. 1). Based on the similar rescue of *dpp* mutants by TkvQD (Fig. 5), it has been proposed that both Sal and Omb expression are initially induced in the anterior stripe of cells, but only Omb expression persists in lineages of these cells via proliferation, generating nested expression of Omb and Sal [44]. In contrast, we show that all the anterior cells are initially a *dpp* source (Fig. 6). Interestingly, a *dpp* source outside the anterior stripe of cells has previously been implicated to control the growth of the entire wing pouch [23], although such a *dpp* source has not been identified and its existence has been questioned [29, 48, 57]. We identified such a *dpp* source contributing to anterior patterning and growth together with the main *dpp* stripe; however, this source does not control growth of the entire wing pouch (Fig. 6, 7).

The non-essential requirement of Dpp dispersal for the anterior compartment is reminiscent of the minor requirement of dispersal of Wg, a morphogen required for wing patterning and growth along the dorsal-ventral axis [11]. It has been shown that a membrane-tethered form of Wg can replace the endogenous Wg without affecting wing patterning and growth [11]. Although the precise requirement of Wg dispersal requires further studies [14], in both cases, transcriptional refinement of each morphogen and persistent signaling by transient morphogen expression allow anterior compartment robust to blocking morphogen dispersal. However, while the *wg* allele encoding a membrane-tethered form is homozygous viable without major phenotypes, ubiquitous blocking of Dpp dispersal by HA trap during development caused lethality (data not shown), indicating a critical role of Dpp dispersal during development. Future studies should reveal the precise role of Dpp dispersal in other developmental processes.

Growth without Dpp dispersal and signaling

Our results also uncover Dpp dispersal- and signaling-independent lateral wing pouch growth once the wing pouch is specified (Fig. 2, 3, 5). How can this be reconciled with the complete loss of wing pouch in classic *dpp* disc alleles (Fig. 5, Extended Data Fig. 3)? The severe phenotypes of *dpp* disc alleles could be due to a failure of the initial specification of the wing pouch [58]. However, the rescue of posterior wing pouch growth in *dpp* mutants by anterior Dpp signaling (Fig. 5) suggests that posterior lateral wing pouch cells can grow without local Dpp signaling upon anterior Dpp signaling activation. Consistently, despite severe growth defects, *5xQE-DsRed* remained expressed in the P compartment upon genetic removal of *tkv* from the entire P compartment from embryonic stages (Extended Data Fig. 7). The non-autonomous posterior growth induction by anterior Dpp signal is not likely caused by juxtaposition of cells with different Dpp signaling level [26]. We thus speculate that, despite a failure of initial wing pouch specification, the posterior lateral wing pouch has the potential to grow but fails to do so in *dpp* disc alleles due to the loss of earlier anterior Dpp signaling. Our results can also explain the previous enigmatic observation that lateral wing fates are less sensitive than medial wing fates in some weak *dpp* mutant alleles [59]. We speculate that in these alleles, *dpp* levels are reduced to a level at which Dpp cannot disperse enough to control posterior patterning and growth but can still activate weak anterior Dpp signaling sufficient to sustain posterior growth.

The presence of Dpp signaling-independent lateral wing pouch growth is unexpected and at odds with all the growth models based on the assumption that Dpp controls overall wing patterning and growth [23-29]. For example, no wing pouch growth is expected without Dpp signaling due to a lack of either a temporal increase of Dpp signaling (temporal model) [60], a detectable Dpp signal (threshold model) [29, 57, 61], or a slope of Dpp signaling activity (gradient model) [24, 25]. Among the models, the best fit model to our observation is the growth equalization model, in which Dpp signaling removes Brk to allow

medial regions to grow, while Brk represses Dpp signaling-independent lateral growth with higher proliferation nature to equalize the non-uniform growth [26, 27]. However, the identity of medial and lateral regions remained undefined in this model. A previous study using morphotrap also identified such a Dpp signaling-insensitive region, but assigned this region to the hinge region due to the severe adult wing growth defects by morphotrap expression [34]. We thus refine the growth equalization model and propose that both medial and lateral regions are located within the wing pouch (Fig. 8b). Consistently, overgrowth phenotypes in *brk* mutant were observed in the wing pouch region rather than in the hinge region (Extended Data Fig. 3). The permissive role of Dpp in modulating a non-uniform growth potential within the wing pouch raises questions about what kind of instructive signals control proliferation and growth, how the non-uniform growth potential emerges independent of Dpp/Brk system [39], as well as how the scaling of patterning with tissue size is achieved.

Conclusion

In developmental biology, interpretational gaps often remain between the mutant phenotypes and the underlying molecular mechanisms. Our approach applying customized protein binder tools to manipulate distinct parameters of Dpp challenges the long-standing dogma that Dpp dispersal controls overall wing patterning and growth, which was not possible by simple mutant analyses, thus demonstrating the utility of the approach to better dissect protein functions during development.

Experimental procedures

Data reporting

No statistical methods were used to predetermine sample size. The experiments were not randomized, and investigators were not blinded to allocation during experiments and outcome assessment.

Fly stocks

Flies were kept in standard fly vials (containing polenta and yeast) in a 25°C incubator. The following fly lines were used: *dpp^{FO}*, *dpp-Gal4*, *UAS-FLP* (Matthew Gibson), *ptc-Gal4* (BL2017), *P{act5C(FRT.polyA)lacZ.nls1}3, ry506* (BL6355), *w[*]; P{w[+mC]=UAS-RedStinger}6, P{w[+mC]=UAS-FLP.Exel}3, P{w[+mC]=Ubi-p63E(FRT.STOP)Stinger}15F2* (G-TRACE)(BL28281), *brk^{XA}* (BL58792), *dpp^{MI03752}* (BL36399), *PBac{RB}e00178, Dp(2;2)DTD48* (Bloomington stock center). *omb*-LacZ (Kyoto101157). *act>Stop, y+>LexA^{LHG}*, *tkv^{a12}*, *UAS-TkvQD*, *pLexAop-TkvQD* (Konrad Basler), *5xQE.DsRed* (Gary Struhl), *UAS/LexAop-HAtrap* (this study), *UAS/LexAop-Dpp trap* (F1) (this study), *dpp^{d8}*, *dpp^{d12}*, *nub-Gal4* (II), *ci-Gal4* (II), *hh-Gal4* (III), *UAS-p35*(III), *tub-Gal80ts* (III) are described from Flybase. *tub>CD2, Stop>Gal4, UAS-nlacZ* (Francesca Pignoni). *TkvHA* (Giorgos Pyrowolakis).

Genotypes by figures

Fig. 1c-e: *yw; HA-dpp/HA-dpp*
Fig. 1g: *yw; ptc-Gal4, Ollas-HA-dpp/+*
Fig. 1i: *yw; ptc-Gal4, Ollas-HA-dpp/+; UAS/LexAop-HAtrap/+*
Fig. 1k: *hsFLP; Ollas-HA-dpp/tub>CD2, Stop>Gal4, UAS-nlacZ; UAS/LexAop-HAtrap/+*
Fig. 1m: *hsFLP; ptc-Gal4, Ollas-HA-dpp/tub>CD2, Stop>Gal4, UAS-nlacZ; UAS/LexAop-HAtrap/+*
Fig. 1o: *hsFLP; Ollas-HA-dpp/tub>CD2, Stop>Gal4, UAS-nlacZ; UAS/LexAop-HAtrap/+*
Fig. 2a, c: (*5xQE.DsRed); ptc-Gal4, HA-dpp/HA-dpp*
Fig. 2b, d: (*5xQE.DsRed); ptc-Gal4, HA-dpp/HA-dpp; UAS/LexAop-HAtrap/+*
Fig. 2k, m: *yw; nub-Gal4, HA-dpp/HA-dpp*
Fig. 2l, n: *yw; nub-Gal4, HA-dpp/HA-dpp; UAS/LexAop-HAtrap/+*
Fig. 3a: *hsFLP/5xQE.DsRed; HA-dpp, tkv^{a12} FRT40/HA-Dpp, UbiGFP, FRT40, ptc-Gal4; UAS/LexAop-HAtrap/+*
Fig. 3b: *hsFLP/5xQE.DsRed; tkv^{a12} FRT40/UbiGFP, FRT40*
Fig. 3c, D: *hsFLP/5xQE.DsRed; tkvHA^{FO}/tkvHA^{FO}*
Fig. 3e, f: (internal control within a cross) *5xQE.DsRed/+; (dpp^{FO}, ci-Gal4)/(dpp^{FO}); (UAS-FLP)/tubGal80ts,*
Fig. 3g, h: *5xQE.DsRed/+; dpp^{FO}, ci-Gal4/dpp^{FO}; UAS-FLP/tubGal80ts,*
Fig. 4b: (left) *yw; ptc-Gal4, Ollas-HA-dpp/+*, (right) *yw; ptc-Gal4, Ollas-HA-dpp/+; UAS/LexAop-Dpptrap/+*
Fig. 4c: *yw; ptc-Gal4, HA-dpp/+*
Fig. 4d: *yw; ptc-Gal4, HA-dpp/+; UAS/LexAop-Dpptrap/+*
Fig. 4k, m: *yw; nub-Gal4, HA-dpp/+*
Fig. 4l, n: *yw; nub-Gal4, HA-dpp/+; UAS/LexAop-Dpptrap/+*
Fig. 5a: (*y)w; dpp^{d8}/dpp^{d12}*
Fig. 5b: (*y)w; dpp^{d8}/dpp^{d12}; dpp-Gal4/UAS-tkvQD*
Fig. 5d: *dpp^{d8}, UAS-FLP/dpp^{d12}, act>Stop, y+>LexA^{LHG}; dpp-Gal4/LexAop-tkvQD* and *5xQE.DsRed/+*; *dpp^{d8}, UAS-FLP/dpp^{d12}, act>Stop, y+>LexA^{LHG}; dpp-Gal4/LexAop-tkvQD*,
Fig. 6b: *yw; dpp-T2A-Gal4, Dp(2;2)DTD48(dpp+)/+; P{w[+mC]=UAS-RedStinger}6, P{w[+mC]=UAS-FLP.Exel}3, P{w[+mC]=Ubi-p63E(FRT.STOP)Stinger}15F2/+*
Fig. 6d-g: *yw M{vas-int.Dm}zh-2A; dpp-T2A-d2GFP-NLS/Cyo, P23*
Fig. 7a-c: *ptc-Gal4, dpp^{FO}/+; tubGal80ts/UAS-FLP, act5C(FRT.polyA)lacZ.nls*

Fig. 7d-h: *ptc-Gal4, dpp^{FO}/dpp^{FO}; tubGal80ts/UAS-FLP, act5C(FRT.polyA)lacZ.nls*
Fig. 7i-j: *ci-Gal4, dpp^{FO}/dpp^{FO}; tubGal80ts/UAS-FLP, act5C(FRT.polyA)lacZ.nls*
Extended Data Fig. 1a: *ptc-Gal4, HA-dpp/HA-dpp*
Extended Data Fig. 1b: *ptc-Gal4, HA-dpp/HA-dpp; UAS/LexAop-HAtrap/+*
Extended Data Fig. 1c: *nub-Gal4, HA-dpp/+; UAS/LexAop-Dpptrap/+*,
Extended Data Fig. 1e: *nub-Gal4, HA-dpp/HA-dpp; UAS/LexAop-HAtrap/+*,
Extended Data Fig. 1f: *nub-Gal4, HA-dpp/HA-dpp; UAS/LexAop-HAtrap/UAS-p35*,
Extended Data Fig. 1h: *nub-Gal4, HA-dpp/+; UAS/LexAop-Dpptrap/+*
Extended Data Fig. 1i: *nub-Gal4, HA-dpp/+; UAS/LexAop-Dpptrap/UAS-p35*, Fig. S3: *nub-Gal4, ptc-Gal4, HA-dpp/HA-dpp*, *nub-Gal4, ptc-Gal4, HA-dpp/HA-dpp; UAS/LexAop-HAtrap/+*
Extended Data Fig. 2a, c, e, g, i: *HA-dpp/HA-dpp, ci>+* (left) and *HA-dpp/HA-dpp, ci>HA* trap (right)
Extended Data Fig. 2k, m, o, q, s: *HA-dpp/+, ci>+* (left) and *HA-dpp/+, ci>Dpp* trap (right)
Extended Data Fig. 3a: *5xQE.DsRed/+, dpp^{d8} or dpp^{d12}/+*
Extended Data Fig. 3b: *5xQE.DsRed/+; dpp^{d8}/dpp^{d12}*
Extended Data Fig. 3c: *5xQE.DsRed, brk^{XA}/Y, dpp^{d8} or dpp^{d12}/+*
Extended Data Fig. 3d: *5xQE.DsRed, brk^{XA}/Y, dpp^{d8}/dpp^{d12}*
Extended Data Fig. 4: (control) *ptc-Gal4, HA-dpp/+*, (Dpptrap) *ptc-Gal4, HA-dpp/+; UAS/LexAop-Dpptrap/+*, (HAtrap) *ptc-Gal4, HA-dpp/HA-dpp; UAS/LexAop-HAtrap/+*
Extended Data Fig. 5: (control) *ptc-Gal4, HA-dpp/HA-dpp; tubGal80ts/+*, (experiment) *ptc-Gal4, HA-dpp/HA-dpp; UAS/LexAop-HAtrap/tubGal80ts*
Extended Data Fig. 6: *tkvHA^{FO}, ci-Gal4/tkvHA^{FO}; UAS-FLP/tubGal80ts*
Extended Data Fig. 7: (control within the cross) *5xQE.DsRed/+; (tkvHA^{FO})/tkvHA^{FO}; (Hh-Gal4)/+* (experiment) *5xQE.DsRed/+; tkvHA^{FO}/tkvHA^{FO}; Hh-Gal4/UAS-FLP*

Immunostainings and antibodies

Protocol as described previously [34]. Each fly cross was set up together with a proper control and genotypes were processed in parallel. If the genotype could be distinguished, experimental and control samples were processed in the same tube. To minimize variations, embryos were staged by collecting eggs for 2-4hrs. An average intensity image from 3 sequential images from a representative wing disc is shown for all the experiments. The following primary antibodies were used; anti-HA (3F10, Roche; 1:300 for conventional staining, 1:20 for extracellular staining), anti-Ollas (Novus Biologicals, 1:300 for conventional staining, 1:20 for extracellular staining), anti-phospho-Smad1/5 (1:200; Cell Signaling), anti-Brk (1:1.000; Gines Morata), anti-Sal (1:500; Rosa Barrio), anti-Omb (1:500; Gert Pflugfelder), anti-Wg (1:120; DSHB, University of Iowa), anti-Ptc (1:40; DSHB, University of Iowa), anti-β-Galactosidase (1:1.000; Promega, 1:1000; abcam). All the primary and secondary antibodies were diluted in 5% normal goat serum (NGS) (Sigma) in PBT (0.03% Triton X-100/PBS). All secondary antibodies from the AlexaFluor series were used at 1:500 dilutions. Wing discs were mounted in Vectashield (H-1000, Vector Laboratories). Images of wing discs were obtained using a Leica TCS SP5 confocal microscope (section thickness 1 μm).

Quantification

Quantification of pMad, Brk, Sal, and Omb

From each z-stack image, signal intensity profile along A/P axis was extracted from average projection of 3 sequential images using ImageJ. Each signal intensity profile was aligned along A/P compartment boundary (based on anti-Ptc staining) and average signal intensity profile from different samples was generated and plotted by the script (wing_disc-alignment.py). The average intensity profile from control and experimental samples were then compared by the script (wingdisc_comparison.py). Both scripts can be obtained from (https://etiennees.github.io/Wing_disc-alignment/). The resulting signal intensity profiles (mean with SD) were generated by Prism.

Quantification of wing pouch size and adult wing size

The A and P compartment of the wing pouches were approximated by Ptc/Wg staining and positions of folds, and the A/P compartment boundary of the adult wings were approximated by L4 position. The size of each compartment was measured using ImageJ. Scatter dot plots (mean with SD) were generated by Prism.

Statistics

Statistical significance was assessed by Prism based on the normality tests using a two-sided Mann-Whitney test (Fig. 2t, for P compartment, Fig. 4s, for A compartment, Fig. 4u, for A compartment) and a two-sided Student's *t*-test with unequal variance for the rest of the comparisons (***p<0.0002 **** p<0.0001).

Generation of *HA-dpp* and *GFP-dpp* knock-in allele

Cloning of plasmids for injection.

A fragment containing multi-cloning sites (MCS) between two inverted attB sites was synthesized and inserted in the pBS (BamHI) vector (from Mario Metzler). A genomic fragment of *dpp* between $dpp^{MI03752}$ and *PBac{RB}e00178* (about 4.4kb), as well as an *FRT* and *3xP3mCherry* were inserted in this MCS by standard cloning procedures. A fragment encoding HA tag or GFP was inserted between the XhoI and NheI sites inserted after the last Furin processing site [17].

Inserting *dpp* genomic fragments in the *dpp* locus

The resulting plasmids were injected in *yw M{vas-int.Dm}zh-2A; $dpp^{MI03752}$/Cyo, P23*. *P23* is a transgene containing a *dpp* genomic fragment to rescue *dpp* haploinsufficiency. After the hatched flies were backcrossed, flies that lost *y* inserted between inverted attP sites in the mimic transposon lines were individually backcrossed to establish stocks. The orientation of inserted fragments was determined by PCR.

Removal of the endogenous *dpp* exon by FLP/FRT recombination

Males from the above stock were crossed with females of genotype *hsFLP; al, PBac{RB}e00178 /SM6, al, sp* and subjected to heat-shock at 37°C for 1hr/day. *PBac{RB}e00178* contains *FRT* sequence and w+ and upon recombination, the *dppHA* genomic fragment are followed by FRT and w+. Hatched males of *hsFLP;dppHA/al,PBac{RB}e00178* were crossed with *yw; al, b, c, sp/ SM6, al, sp*. From this cross, flies *yw; dppHA(w+)/SM6, al, sp* were individually crossed with *yw; al, b, c, sp/ SM6, al, sp* to establish the stock.

Construction of α-HAscFv

cDNA of HAscFv was constructed by combining coding sequences of variable regions of the heavy chain (V_H: 1-423 of LC522514) and of the light chain (V_L: 67-420 of LC522515) cloned from anti-HA hybridoma (clone 12CA5 [62]) with a linker sequence (5'-accggtGGCGGAGGCTCTGGCGGAGGAGGTTCCGGCGGAGGTGGAAGCgatatc-3') in the order of V_H-linker-V_L. The coding sequence of HAscFv was cloned into pCS2+mcs-2FT-T for FLAG-tagging. Requests for HAscFv should be addressed to YM (mii@nibb.ac.jp). To generate HA trap, the region encoding morphotrap (VHH-GFP4) was replaced with KpnI and SphI sites in pLOTattB-VHH-GFP4:CD8-mChery [34]. A fragment encoding HAscFv was amplified by PCR and then inserted via KpnI and SphI sites by standard cloning procedures.

Selection of Dpp-binding DARPins and generation of Dpp trap

Streptavidin-binding peptide (SBP)-tagged mature C-terminal domain of Dpp was cloned into pRSFDuet vector by a standard cloning. Dpp was overexpressed in *E. coli*, extracted from inclusion bodies, refolded, and purified by heparin affinity chromatography followed by reverse phase HPLC [63]. To isolate suitable DARPins, SBP-tagged Dpp was immobilized on streptavidin magnetic beads and used as a target for DARPin selections by employing multiple rounds of Ribosome Display [64, 65]. Due

to the aggregation and precipitation propensity of the purified SBP-Dpp, the refolded dimers previously stored in 6 M urea buffer (6 M urea, 50 mM Tris-HCl, 2 mM EDTA pH8.0, 0.25 M NaCl) were diluted to a concentration of 100-120 µg/ml in the same buffer and subsequently dialyzed against 4 mM HCl at 4°C overnight. To ensure binding of correctly folded Dpp to the beads, this solution was diluted five times in the used selection buffer just prior to bead loading and the start of the ribosome display selection. In each panning round, the target concentration presented on magnetic beads was reduced, while the washing stringency was simultaneously increased to enrich for binders with high affinities [65]. In addition, from the second round onward, a pre-panning against Streptavidin beads was performed prior to the real selection to reduce the amounts of matrix binders. After four rounds of selection, the enriched pool was cloned into an *E. coli* expression vector, enabling the production of both N-terminally His_8- and C-terminally FLAG-tagged DARPins. Nearly 400 colonies of transformed *E. coli* were picked and the encoded binders expressed in small scale. Bacterial crude extracts were subsequently used in enzyme-linked immunosorbent assay (ELISA) screenings, detecting the binding of candidate DARPins to streptavidin-immobilized Dpp, or just streptavidin (indicating background binding) by using a FLAG-tag based detection system (data not shown). Of those 127 candidate DARPins interacting with streptavidin-immobilized Dpp, 73 (or 57%) specifically bound to Dpp (i.e., having at least threefold higher signal for streptavidin-immobilized Dpp than to streptavidin alone). 36 of these (50%) revealed unique and full-length sequences. To generate Dpp trap, the region encoding morphotrap (VHH-GFP4) was replaced with KpnI and SphI sites in pLOTattB-VHH-GFP4:CD8-mChery [34]. Each fragment encoding a DARPin was amplified by PCR and then inserted via KpnI and SphI sites by standard cloning procedures.

Generation of *tkvHA^{FO}* (Flip-out) allele

The *tkvHA* allele was previously described [66]. An FRT cassette was inserted in the re-insertion vector for *tkvHA* (Genewiz) and re-inserted into the attP site in the *tkv* locus.

Generation of endogenous *dpp-Gal4*

pBS-KS-attB2-SA(1)-T2A-Gal4-Hsp70 (addgene 62897) was injected in the *yw M{vas-int.Dm}zh-2A; dpp^{MI03752}/Cyo, P23* stock. Since the *Gal4* insertion causes haploinsufficiency, the *dpp-Gal4* was recombined with *Dp(2;2)DTD48* (duplication of *dpp*) for G-TRACE analysis.

Generation of an endogenous *dpp* reporter

A DNA fragment containing T2A-d2GFP-NLS was synthesized and used to replace the region containing *T2A-Gal4* in *pBS-KS-attB2-SA(1)-T2A-Gal4-Hsp70* via BamHI to generate *pBS-KS-attB2-SA(1)-T2A-d2GFP-NLS-Hsp70* (Genewiz). The resulting plasmid was injected in the *yw M{vas-int.Dm}zh-2A; dpp^{MI03752}/ Cyo, P23* stock.

Acknowledgments:
We thank Konrad Basler, Giorgos Pyrowolakis, Gustavo Aguilar, and Sheida Hadji Rasouliha for comments on the manuscript. Stocks obtained from the Bloomington Drosophila Stock Center (NIH P40OD018537) were used in this study. We thank Konrad Basler, Gary Struhl, Matthew Gibson, Giorgos Pyrowolakis, and Kyoto stock center for flies. We thank Gines Morata, Rosa Barrio, Gert Pflugfelder, and the Developmental Studies Hybridoma Bank at The University of Iowa for antibodies. We thank the Biozentrum Imaging Core Facility for maintenance of microscopes and support. We thank Etienne Schmelzer for scripts for quantification and Oguz Kanca for the idea to manipulate *dpp* locus. We would like to thank Bernadette Bruno, Gina Evora and Karin Mauro for constant and reliable supply with world's best fly food. We further acknowledge all current and former members of the High-Throughput Binder Selection facility at the Department of Biochemistry of the University of Zurich for their contribution to the establishment of the semi-automated ribosome display that resulted in the generation of the used anti-Dpp DARPin binders, particularly Thomas Reinberg. **Funding:** SM has been supported by a JSPS Postdoctoral Fellowship for Research Abroad and the Research Fund Junior Researchers University of Basel, and is currently supported by a SNSF Ambizione grant (PZ00P3_180019). YM has been supported by JST PRESTO (JPMJPR194B) and JSPS KAKENHI (18K14720). The work in the Affolter laboratory was supported by grants from Kantons Basel-Stadt and Basel-Land and from the SNSF (MA).

Author contributions: This project was conceived by SM and MA. SM designed, performed, and analyzed all the experiments. JVS and AP isolated DARPins against Dpp. YM, YH, and MT cloned α-HA scFv. DB helped with Dpp purification. The main text was written by SM and MA with comments from all the authors.

Competing interests: Authors declare no competing interests.

References

1. Helma, J., Cardoso, M. C., Muyldermans, S. & Leonhardt, H. Nanobodies and recombinant binders in cell biology. *J. Cell Biol.* **209**, 633-644 (2015).
2. Harmansa, S. & Affolter, M. Protein binders and their applications in developmental biology. *Development* **145**, 10.1242/dev.148874 (2018).
3. Bieli, D. *et al*. Development and Application of Functionalized Protein Binders in Multicellular Organisms. *Int. Rev. Cell. Mol. Biol.* **325**, 181-213 (2016).
4. Kaiser, P. D., Maier, J., Traenkle, B., Emele, F. & Rothbauer, U. Recent progress in generating intracellular functional antibody fragments to target and trace cellular components in living cells. *Biochim. Biophys. Acta* **1844**, 1933-1942 (2014).
5. Turing, A. The chemical basis of morphogenesis. *Philosophical Transactions of the Royal Society of London B* **237** (1952).
6. Tabata, T. Genetics of morphogen gradients. *Nat. Rev. Genet.* **2**, 620-630 (2001).
7. Ashe, H. L. & Briscoe, J. The interpretation of morphogen gradients. *Development* **133**, 385-394 (2006).
8. Rogers, K. W. & Schier, A. F. Morphogen gradients: from generation to interpretation. *Annu. Rev. Cell Dev. Biol.* **27**, 377-407 (2011).
9. Kicheva, A., Bollenbach, T., Wartlick, O., Julicher, F. & Gonzalez-Gaitan, M. Investigating the principles of morphogen gradient formation: from tissues to cells. *Curr. Opin. Genet. Dev.* **22**, 527-532 (2012).
10. Sagner, A. & Briscoe, J. Morphogen interpretation: concentration, time, competence, and signaling dynamics. *Wiley Interdiscip. Rev. Dev. Biol.* **6**, 10.1002/wdev.271. Epub 2017 Mar 20 (2017).
11. Alexandre, C., Baena-Lopez, A. & Vincent, J. P. Patterning and growth control by membrane-tethered Wingless. *Nature* **505**, 180-185 (2014).
12. Tian, A., Duwadi, D., Benchabane, H. & Ahmed, Y. Essential long-range action of Wingless/Wnt in adult intestinal compartmentalization. *PLoS Genet.* **15**, e1008111 (2019).
13. Apitz, H. & Salecker, I. Spatio-temporal relays control layer identity of direction-selective neuron subtypes in Drosophila. *Nat. Commun.* **9**, 2295-018-04592-z (2018).
14. Chaudhary, V. *et al*. Robust Wnt signaling is maintained by a Wg protein gradient and Fz2 receptor activity in the developing Drosophila wing. *Development* **146**, 10.1242/dev.174789 (2019).
15. Resino, J., Salama-Cohen, P. & Garcia-Bellido, A. Determining the role of patterned cell proliferation in the shape and size of the Drosophila wing. *Proc. Natl. Acad. Sci. U. S. A.* **99**, 7502-7507 (2002).
16. Entchev, E. V., Schwabedissen, A. & Gonzalez-Gaitan, M. Gradient formation of the TGF-beta homolog Dpp. *Cell* **103**, 981-991 (2000).
17. Teleman, A. A. & Cohen, S. M. Dpp gradient formation in the Drosophila wing imaginal disc. *Cell* **103**, 971-980 (2000).
18. Affolter, M. & Basler, K. The Decapentaplegic morphogen gradient: from pattern formation to growth regulation. *Nat. Rev. Genet.* **8**, 663-674 (2007).
19. Zhou, S. *et al*. Free extracellular diffusion creates the Dpp morphogen gradient of the Drosophila wing disc. *Curr. Biol.* **22**, 668-675 (2012).
20. Belenkaya, T. Y. *et al*. Drosophila Dpp morphogen movement is independent of dynamin-mediated endocytosis but regulated by the glypican members of heparan sulfate proteoglycans. *Cell* **119**, 231-244 (2004).
21. Schwank, G. *et al*. Formation of the long range Dpp morphogen gradient. *PLoS Biol.* **9**, e1001111 (2011).
22. Hsiung, F., Ramirez-Weber, F. A., Iwaki, D. D. & Kornberg, T. B. Dependence of Drosophila wing imaginal disc cytonemes on Decapentaplegic. *Nature* **437**, 560-563 (2005).

614 23. Akiyama, T. & Gibson, M. C. Decapentaplegic and growth control in the developing Drosophila
615 wing. *Nature* **527**, 375-378 (2015).
616 24. Rogulja, D. & Irvine, K. D. Regulation of cell proliferation by a morphogen gradient. *Cell* **123**,
617 449-461 (2005).
618 25. Rogulja, D., Rauskolb, C. & Irvine, K. D. Morphogen control of wing growth through the Fat
619 signaling pathway. *Dev. Cell.* **15**, 309-321 (2008).
620 26. Schwank, G., Restrepo, S. & Basler, K. Growth regulation by Dpp: an essential role for Brinker
621 and a non-essential role for graded signaling levels. *Development* **135**, 4003-4013 (2008).
622 27. Schwank, G. *et al*. Antagonistic growth regulation by Dpp and Fat drives uniform cell
623 proliferation. *Dev. Cell.* **20**, 123-130 (2011).
624 28. Wartlick, O., Mumcu, P., Jülicher, F. & Gonzalez-Gaitan, M. Response to Comment on
625 "Dynamics of Dpp Signaling and Proliferation Control". *Science* **335**, 401 (2012).
626 29. Bosch, P. S., Ziukaite, R., Alexandre, C., Basler, K. & Vincent, J. P. Dpp controls growth and
627 patterning in Drosophila wing precursors through distinct modes of action. *Elife* **6**,
628 10.7554/eLife.22546 (2017).
629 30. Zhu, Y., Qiu, Y., Chen, W., Nie, Q. & Lander, A. D. Scaling a Dpp Morphogen Gradient through
630 Feedback Control of Receptors and Co-receptors. *Dev. Cell.* **53**, 724-739.e14 (2020).
631 31. Ben-Zvi, D., Pyrowolakis, G., Barkai, N. & Shilo, B. Z. Expansion-repression mechanism for
632 scaling the Dpp activation gradient in Drosophila wing imaginal discs. *Curr. Biol.* **21**, 1391-1396
633 (2011).
634 32. Hamaratoglu, F., de Lachapelle, A. M., Pyrowolakis, G., Bergmann, S. & Affolter, M. Dpp
635 signaling activity requires Pentagone to scale with tissue size in the growing Drosophila wing
636 imaginal disc. *PLoS Biol.* **9**, e1001182 (2011).
637 33. Wartlick, O. *et al*. Dynamics of Dpp signaling and proliferation control. *Science* **331**, 1154-1159
638 (2011).
639 34. Harmansa, S., Hamaratoglu, F., Affolter, M. & Caussinus, E. Dpp spreading is required for
640 medial but not for lateral wing disc growth. *Nature* **527**, 317-322 (2015).
641 35. Venken, K. J. *et al*. MiMIC: a highly versatile transposon insertion resource for engineering
642 Drosophila melanogaster genes. *Nat. Methods* **8**, 737-743 (2011).
643 36. Akiyama, T. & Gibson, M. C. Morphogen transport: theoretical and experimental controversies.
644 *Wiley Interdiscip. Rev. Dev. Biol.* **4**, 99-112 (2015).
645 37. Kicheva, A. & Gonzalez-Gaitan, M. The Decapentaplegic morphogen gradient: a precise
646 definition. *Curr. Opin. Cell Biol.* **20**, 137-143 (2008).
647 38. Matsuda, S., Harmansa, S. & Affolter, M. BMP morphogen gradients in flies. *Cytokine Growth*
648 *Factor Rev.* **27**, 119-127 (2016).
649 39. Restrepo, S., Zartman, J. J. & Basler, K. Coordination of patterning and growth by the
650 morphogen DPP. *Curr. Biol.* **24**, R245-55 (2014).
651 40. Burke, R. & Basler, K. Dpp receptors are autonomously required for cell proliferation in the
652 entire developing Drosophila wing. *Development* **122**, 2261-2269 (1996).
653 41. Kim, J., Johnson, K., Chen, H. J., Carroll, S. & Laughon, A. Drosophila Mad binds to DNA and
654 directly mediates activation of vestigial by Decapentaplegic. *Nature* **388**, 304-308 (1997).
655 42. Nellen, D., Affolter, M. & Basler, K. Receptor serine/threonine kinases implicated in the control
656 of Drosophila body pattern by decapentaplegic. *Cell* **78**, 225-237 (1994).
657 43. Nellen, D., Burke, R., Struhl, G. & Basler, K. Direct and long-range action of a DPP morphogen
658 gradient. *Cell* **85**, 357-368 (1996).
659 44. Lecuit, T. *et al*. Two distinct mechanisms for long-range patterning by Decapentaplegic in the
660 Drosophila wing. *Nature* **381**, 387-393 (1996).
661 45. Matsuda, S. & Shimmi, O. Directional transport and active retention of Dpp/BMP create wing
662 vein patterns in Drosophila. *Dev. Biol.* **366**, 153-162 (2012).

663 46. Pluckthun, A. Designed ankyrin repeat proteins (DARPins): binding proteins for research,
664 diagnostics, and therapy. *Annu. Rev. Pharmacol. Toxicol.* **55**, 489-511 (2015).
665 47. Evans, C. J. *et al*. G-TRACE: rapid Gal4-based cell lineage analysis in Drosophila. *Nat. Methods*
666 **6**, 603-605 (2009).
667 48. Matsuda, S. & Affolter, M. Dpp from the anterior stripe of cells is crucial for the growth of the
668 Drosophila wing disc. *Elife* **6**, 10.7554/eLife.22319 (2017).
669 49. Aguilar, G., Vigano, M. A., Affolter, M. & Matsuda, S. Reflections on the use of protein binders
670 to study protein function in developmental biology. *Wiley interdisciplinary reviews.Developmental*
671 *biology*, e356 (2019).
672 50. Boersma, S. *et al*. Multi-Color Single-Molecule Imaging Uncovers Extensive Heterogeneity in
673 mRNA Decoding. *Cell* **178**, 458-472.e19 (2019).
674 51. Gotzke, H. *et al*. The ALFA-tag is a highly versatile tool for nanobody-based bioscience
675 applications. *Nat. Commun.* **10**, 4403-019-12301-7 (2019).
676 52. Tanenbaum, M. E., Gilbert, L. A., Qi, L. S., Weissman, J. S. & Vale, R. D. A protein-tagging
677 system for signal amplification in gene expression and fluorescence imaging. *Cell* **159**, 635-646
678 (2014).
679 53. Zhao, N. *et al*. A genetically encoded probe for imaging nascent and mature HA-tagged proteins
680 in vivo. *Nat. Commun.* **10**, 2947-019-10846-1 (2019).
681 54. Adachi-Yamada, T., Fujimura-Kamada, K., Nishida, Y. & Matsumoto, K. Distortion of
682 proximodistal information causes JNK-dependent apoptosis in Drosophila wing. *Nature* **400**, 166-
683 169 (1999).
684 55. Adachi-Yamada, T. & O'Connor, M. B. Morphogenetic apoptosis: a mechanism for correcting
685 discontinuities in morphogen gradients. *Dev. Biol.* **251**, 74-90 (2002).
686 56. Akiyama, T., User, S. D. & Gibson, M. C. Somatic clones heterozygous for recessive disease
687 alleles of BMPR1A exhibit unexpected phenotypes in Drosophila. *Elife* **7**, 10.7554/eLife.35258
688 (2018).
689 57. Barrio, L. & Milan, M. Boundary Dpp promotes growth of medial and lateral regions of the
690 Drosophila wing. *Elife* **6**, 10.7554/eLife.22013 (2017).
691 58. Paul, L. *et al*. Dpp-induced Egfr signaling triggers postembryonic wing development in
692 Drosophila. *Proc. Natl. Acad. Sci. U. S. A.* **110**, 5058-5063 (2013).
693 59. Bangi, E. & Wharton, K. Dpp and Gbb exhibit different effective ranges in the establishment of
694 the BMP activity gradient critical for Drosophila wing patterning. *Dev. Biol.* **295**, 178-193 (2006).
695 60. Wartlick, O. *et al*. Dynamics of Dpp signaling and proliferation control. *Science* **331**, 1154-1159
696 (2011).
697 61. Barrio, L. & Milan, M. Regulation of Anisotropic Tissue Growth by Two Orthogonal Signaling
698 Centers. *Dev. Cell.* **52**, 659-672.e3 (2020).
699 62. Mii, Y et al., https://www.biorxiv.org/content/10.1101/2020.02.20.957860v1
700 63. Groppe, J. *et al*. Biochemical and biophysical characterization of refolded Drosophila DPP, a
701 homolog of bone morphogenetic proteins 2 and 4. *J. Biol. Chem.* **273**, 29052-29065 (1998).
702 64. Pluckthun, A. Ribosome display: a perspective. *Methods Mol. Biol.* **805**, 3-28 (2012).
703 65. Dreier, B. & Pluckthun, A. Rapid selection of high-affinity binders using ribosome display.
704 *Methods Mol. Biol.* **805**, 261-286 (2012).
705 66. Norman, M., Vuilleumier, R., Springhorn, A., Gawlik, J. & Pyrowolakis, G. Pentagone
706 internalises glypicans to fine-tune multiple signalling pathways. *Elife* **5**, 10.7554/eLife.13301 (2016).
707

Fig. 1

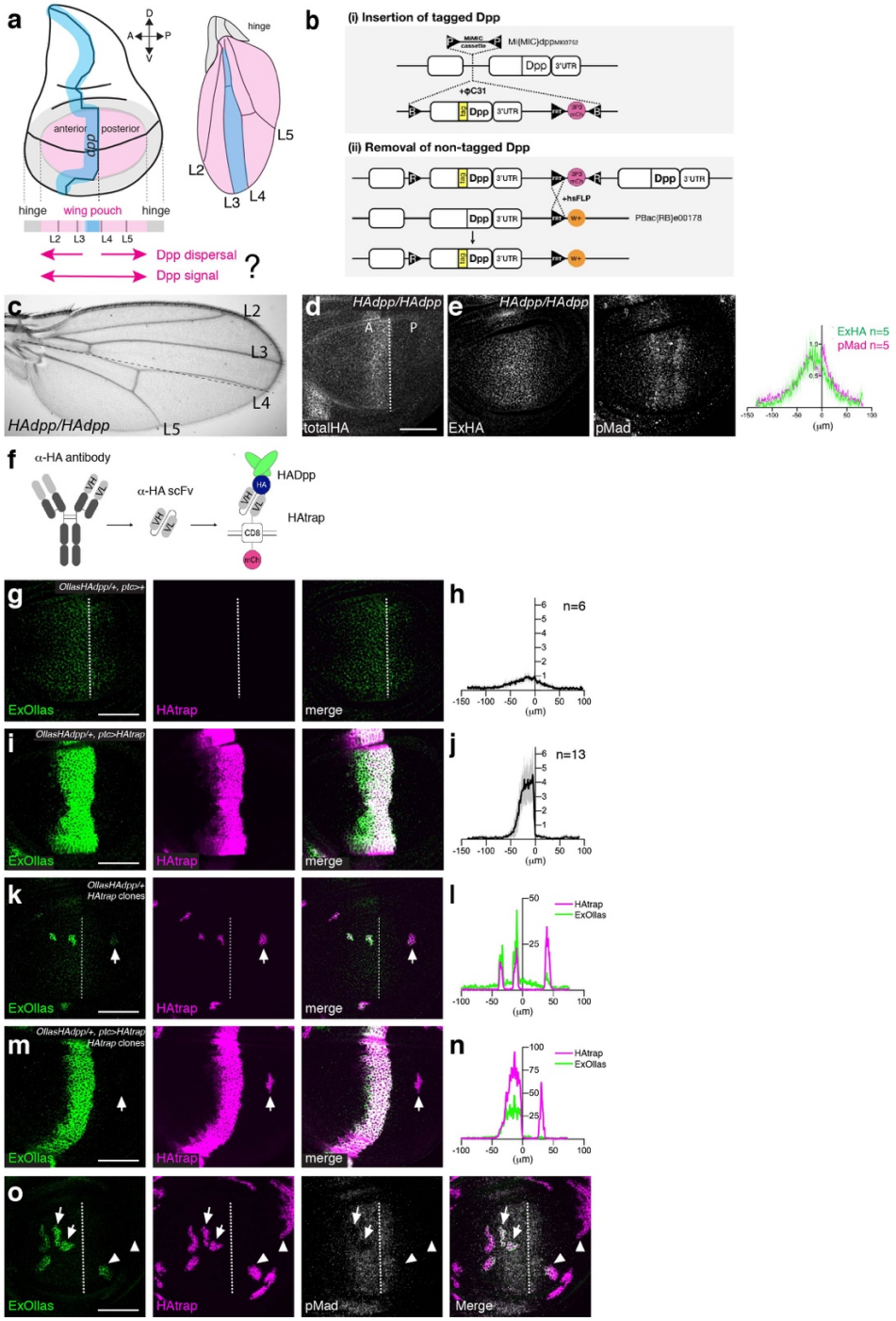

Figure 1. Generation and characterization of HA trap

a, A schematic view of the wing disc and the adult wing. **b**, A schematic view of a platform manipulating endogenous *dpp* locus. **c**, Adult wing of a homozygous *HA-dpp* fly. **d**, α-HA staining of *HA-dpp* homozygous wing disc. **e**, α-ExHA and α-pMad staining of *HA-dpp* homozygous wing disc. Quantification of each staining. **f**, A schematic view of HA trap. **g**, α-ExOllas, HA trap, and merge of control *Ollas-HA-dpp*/+ wing disc. **h**, Quantification of α-ExOllas staining of (**g**). **i**, α-ExOllas, HA trap, and merge of *Ollas-HA-dpp*/+ wing disc expressing HA trap using *ptc-Gal4*. **j**, Quantification of α-ExOllas staining of (**i**). **k**, α-ExOllas, HA trap, and merge of *Ollas-HA-dpp*/+ wing disc expressing HA trap clones. **l**, Quantification of α-ExOllas and HA trap staining of (**k**). **m**, α-ExOllas, HA trap, and merge of *Ollas-HA-dpp*/+ wing disc wing disc expressing HA trap using ptc-Gal4 as well as HA trap clones. **n** Quantification of α-ExOllas and HA trap staining of (**m**). **o**, α-ExOllas, HA trap, pMad and merge of *Ollas-HA-dpp*/+ wing disc expressing HA trap clones. Dashed white lines mark the A-P compartment border. Scale bar 50 μm.

Fig. 2

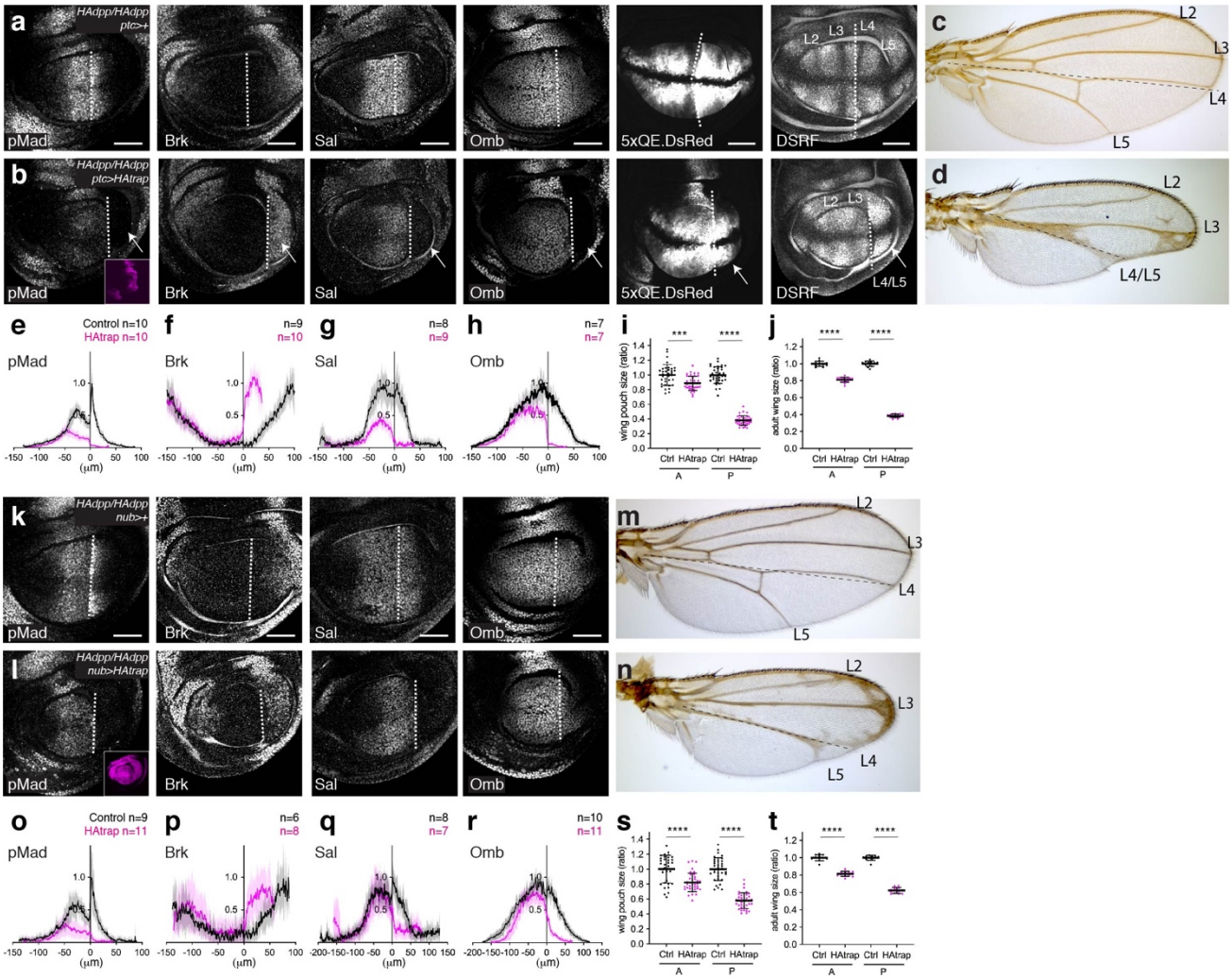

Figure 2. Blocking Dpp dispersal by HA trap causes minor and asymmetric patterning and growth defects

a-**b**, α-pMad, α-Brk, α-Sal, α-Omb, 5xQE.DsRed, DSRF, and Dpp trap (mCherry) (inset) of control wing disc (**a**) and wing disc expressing HA trap using *ptc-Gal4* (**b**). **c**-**d**, Control adult wing (**c**), and adult wing expressing HA trap using *ptc-Gal4* (**d**). **e**-**h**, Quantification of α-pMad (**e**), α-Brk (**f**), α-Sal (**g**), α-Omb (**h**) staining in (**a**-**b**). **i**-**j**, Quantification of compartment size of wing pouch (**i**) and adult wing (**j**) upon HA trap expression using *ptc-Gal4*. **k**-**l**, α-pMad, α-Brk, α-Sal, α-Omb, 5xQE.DsRed, DSRF, and Dpp trap (mCherry) (inset) of control wing disc (**k**) and wing disc expressing HA trap using *nub-Gal4* (**l**). **m**-**n**, Control adult wing (**m**) and adult wing expressing HA trap using *nub-Gal4* (**n**). **o**-**r**, Quantification of α-pMad (**o**), α-Brk (**p**), α-Sal (**q**), α-Omb (**r**) staining in (**k**-**l**). **s**-**t**, Quantification of compartment size of wing pouch (**s**) and adult wing (**t**) upon HA trap expression using *nub-Gal4*. Dashed white lines mark the A-P compartment border. Scale bar 50 μm.

Fig.3

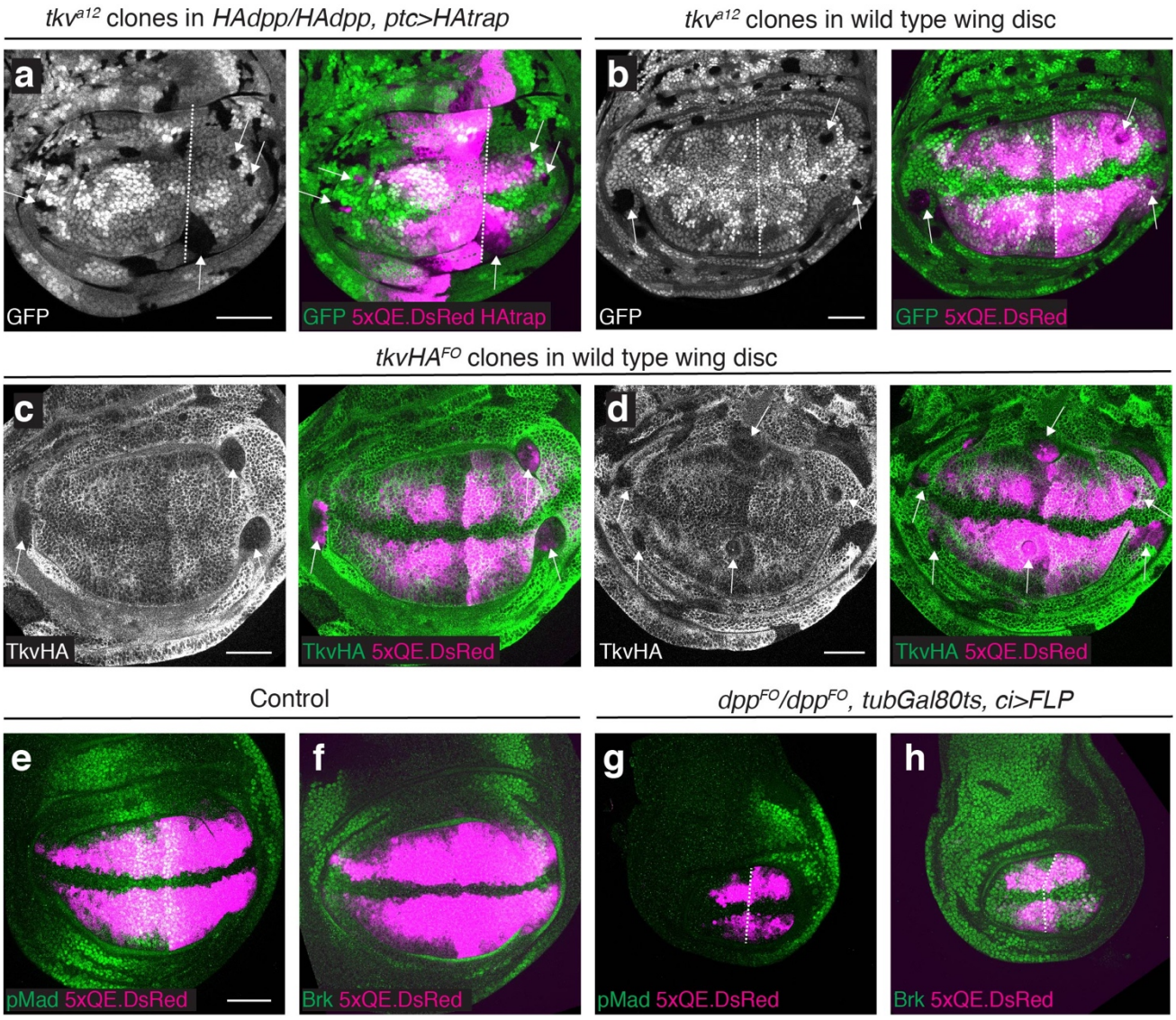

Figure 3. Lateral wing pouch growth without Dpp signaling

a-**b**, *tkv*^{a12} clones (indicated by the absence of GFP signal) induced in *HA-dpp/HA-dpp, ptc>HA* trap wing discs (**a**) and in wild type wing discs (**b**). **c**-**d**, *tkvHA*^{FO} clones (indicated by the absence of α-HA staining) in wild type wing discs. Clones were induced at 60-72 hr AEL (after egg laying) during mid-second to early third instar stages. **e**-**h**, α-pMad and 5xQE.DsRed (**e**, **g**) and α-Brk and 5xQE.DsRed (**f**, **h**) of control wing disc (**e**, **f**) and wing disc removing *dpp* using *ci-Gal4* with *tubGal80s* (**g**, **h**). Crosses were shifted from 18°C to 29°C at 4day AEL (early second instar). Scale bar 50 μm.

Fig.4

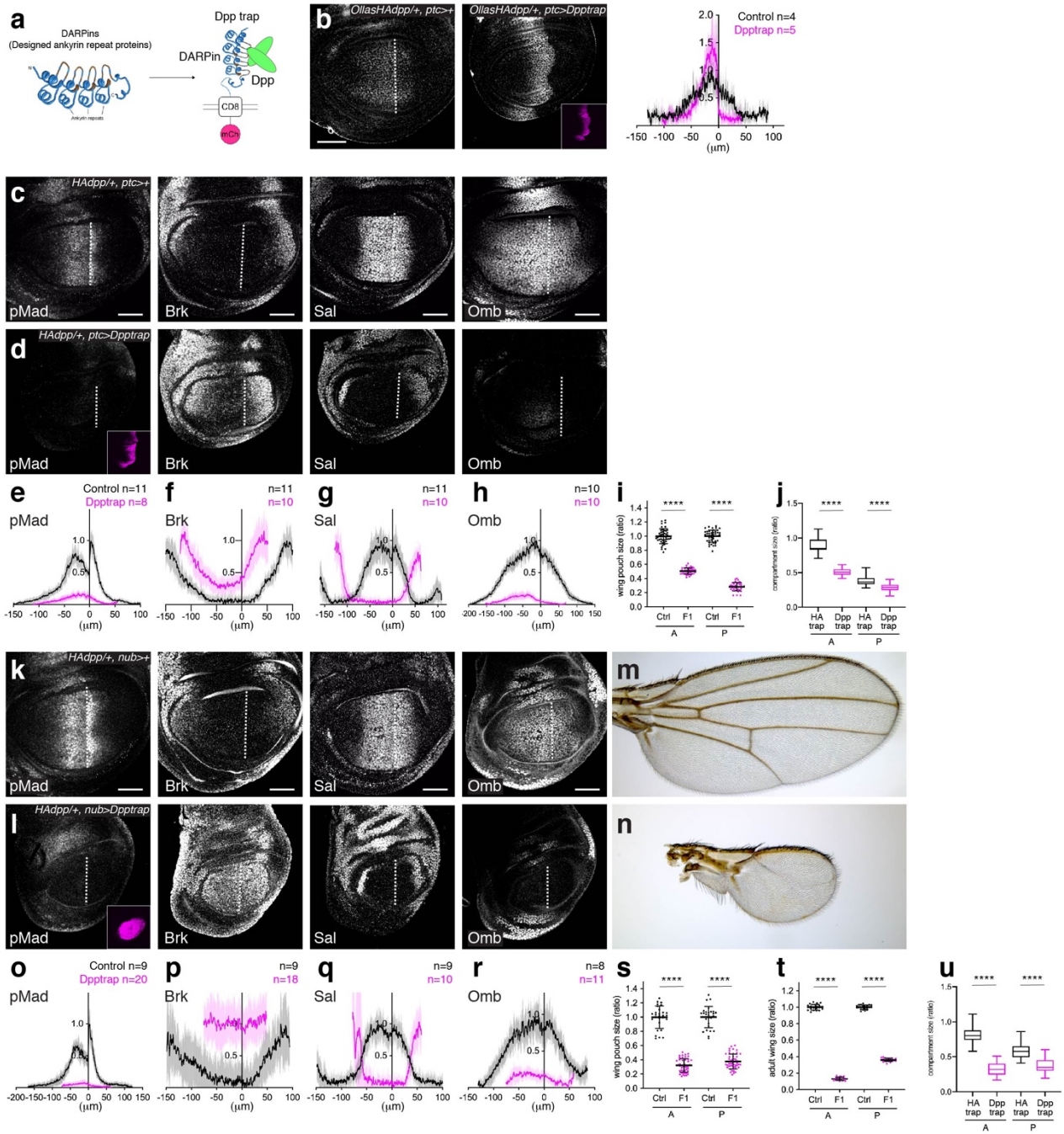

Figure 4. Blocking Dpp dispersal and signaling by Dpp trap causes severe defects similar to *dpp* mutant

a, a schematic view of Dpp trap based on DARPins [2] against Dpp. **b**, α-ExOllas staining and Dpp trap expression (mCherry) (inset) of control wing disc (left) and wing disc expressing Dpp trap using *ptc-Gal4* (right). Quantification of ExOllas signal. **c-d**, α-pMad, α-Brk, α-Sal, α-Omb staining and Dpp trap (mCherry) expression (inset) of control wing disc (**c**) and wing disc expressing Dpp trap using *ptc-Gal4* (**d**). **e-h**, Quantification of α-pMad (**e**), α-Brk (**f**), α-Sal (**g**), α-Omb (**h**) staining in (**c-d**). **i**, Quantification of compartment size of wing pouch upon Dpp trap expression using *ptc-Gal4*. **j**, Comparison of wing pouch compartment size upon HA trap and Dpp trap expression using *ptc-Gal4* (comparison of Fig. 2i and Fig. 4i). **k-l**, α-pMad, α-Brk, α-Sal, α-Omb staining and Dpp trap (mCherry) expression (inset) of control wing disc (**k**) and wing disc expressing Dpp trap using *nub-Gal4* (**l**). **m-n**, Control adult wing (**m**), and adult wing expressing Dpp trap using *nub-Gal4* (**n**). **o-r**, Quantification of α-pMad (**o**), α-Brk (**p**), α-Sal (**q**), α-Omb (**r**) staining in (**k-l**). **s-t**, Quantification of compartment size of wing pouch (**s**) and adult wing (**t**) upon Dpp trap expression using *nub-Gal4*. **u**, Comparison of compartment size of wing pouch upon HA trap and Dpp trap expression using *nub-Gal4* (comparison of Fig. 2s and Fig. 4s). Scale bar 50 μm.

Fig.5

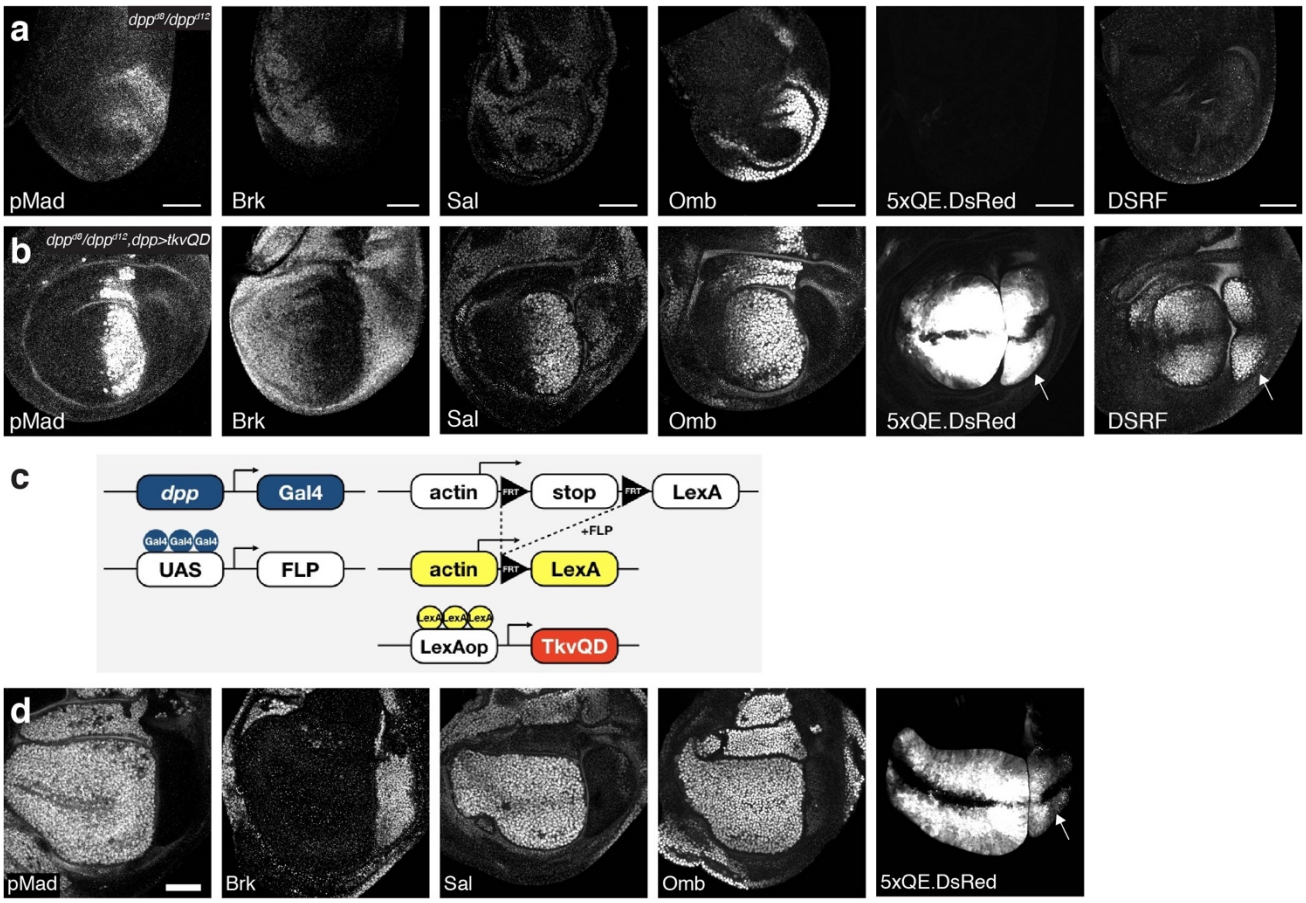

Figure. 5 Rescue of *dpp* mutant by cell-autonomous Dpp signaling mimics phenotypes caused by HA trap

a-**b**, α-pMad, α-Brk, α-Sal, α-Omb, 5xQE.DsRed, and DSRF staining of (**a**) *dpp*$^{d8/d12}$ wing disc and (**b**) *dpp*$^{d8/d12}$*, dpp>tkvQD* wing disc. **c**, A schematic view of converting *dpp-Gal4* into a *LexA* driver, which is permanently expressed in lineages of *dpp-Gal4* expressing cells. In this experimental setup, the lineages of *dpp-Gal4* (including lineages of non-specific *dpp-Gal4* expression) will permanently activate TkvQD and thus pMad signaling. **d**, α-pMad, α-Brk, α-Sal, α-Omb staining, and *5xQE.DsRed* signal of *dpp*^{d8}/*dpp*^{d12}*, dpp-Gal4>UAS-FLP, act>y+>LexA-LHG, LOP-tkvQD* wing disc. Arrows indicate posterior wing pouch growth rescued by anterior Dpp signaling. Scale bar 50 μm. Note that while uniformly upregulated in the A compartment, pMad (which reflects the lineages of *dpp-Gal4*) was absent in the P compartment. Nevertheless, the *5xQE.DsRed* reporter was still activated in both compartments.

Fig.6

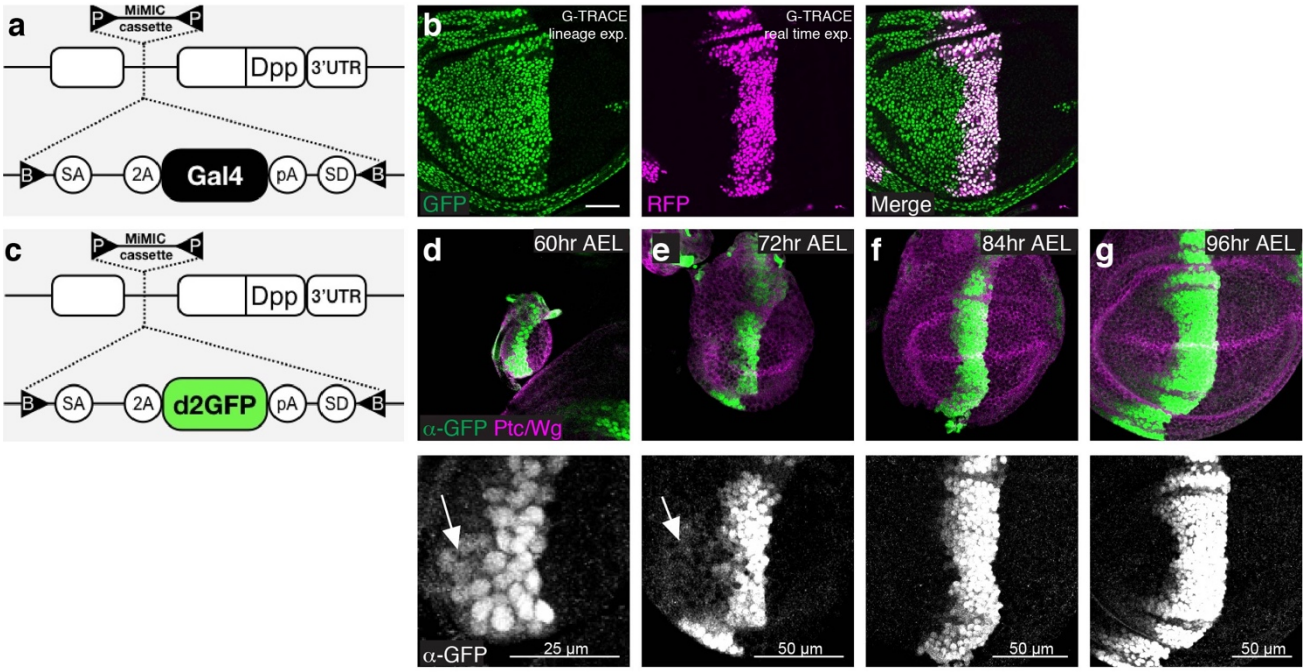

Figure 6. Initial uniform *dpp* transcription in the anterior compartment

a-e, *dpp* transcription dynamics during wing development. (**a**) a schematic view of *d2GFP* insertion into the *dpp* locus. (**b-e**) α-GFP and α-Ptc/Wg staining of wing disc expressing the *d2GFP* reporter at mid-second instar stage (60hr AEL) (**b**), at early third instar stage (72hr AEL) (**c**), at mid-third instar stage (84hr AEL) (**d**) at mid- to late- third instar stage (96hr AEL) (**e**). Arrow indicates *dpp* transcription outside the stripe of cells. **f-g**, Lineages of endogenous *dpp-Gal4* during wing development. **f**, a schematic view of a *Gal4* insertion into the *dpp* locus. **g**, G-TRACE analysis of the endogenous *dpp-Gal4.* Scale bar 50 μm unless otherwise mentioned.

Fig.7

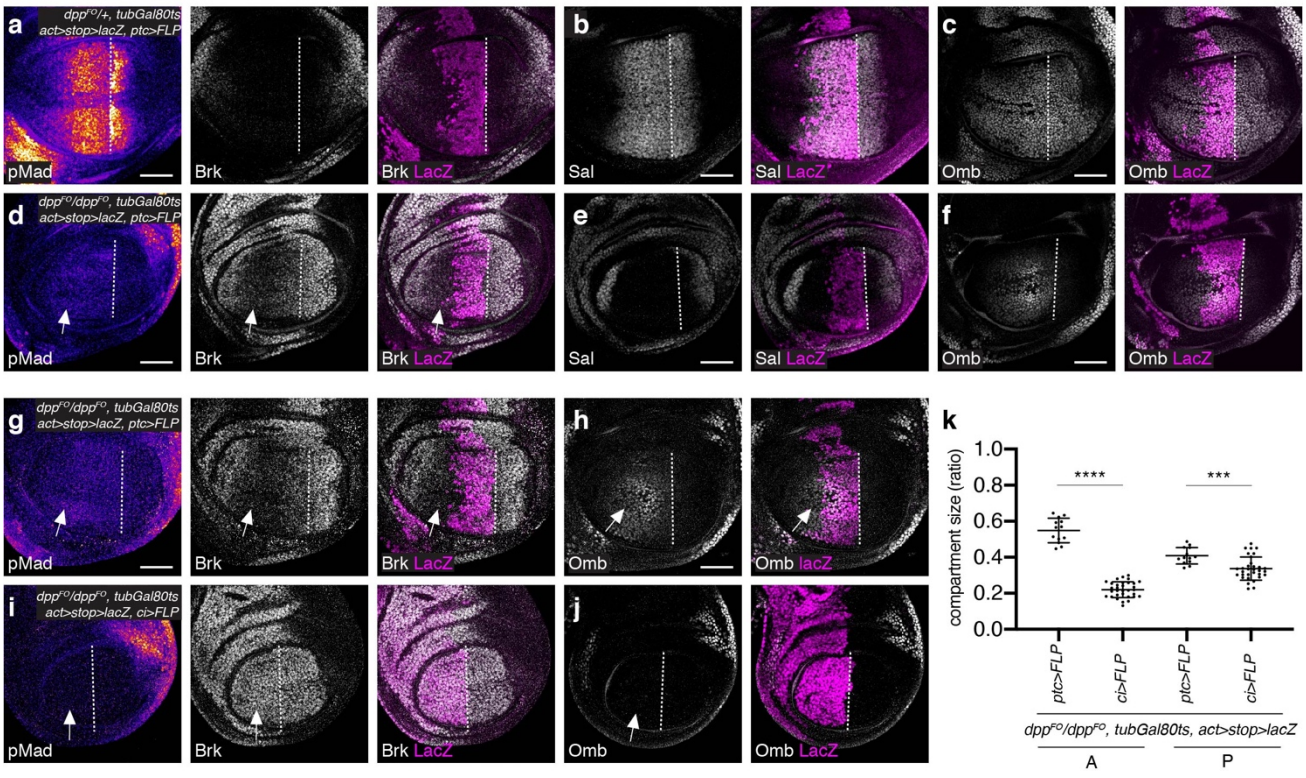

Figure 7. Transient anterior *dpp* source outside Sal domain is required for anterior patterning and growth

a-f, α-pMad, α-Brk, and α-LacZ (**a**, **d**), α-Sal and α-LacZ (**b**, **e**), α-Omb and α-LacZ (**c**, **f**) staining of control wing disc (**a**-**c**) and wing discs removing *dpp* using *ptc-Gal4* from mid-second instar (**d**-**f**). **g**-**j**, α-pMad, α-Brk, and α-LacZ (**g**, **i**), α-Omb and α-LacZ (**h**, **j**) staining of wing disc removing *dpp* using *ptc-Gal4* (**g**, **h**) and using *ci-Gal4* (**i**, **j**) from mid-second instar. **k**, Quantification of each compartment size of wing discs removing *dpp* using *ptc-Gal4* or *ci-Gal4*. Crosses were shifted from 18°C to 29°C at 5day AEL (mid-second instar). α-LacZ staining marks the region where *dpp* is removed upon FLP expression. Dashed white lines mark the A-P compartment border. Scale bar 50 μm.

Fig. 8

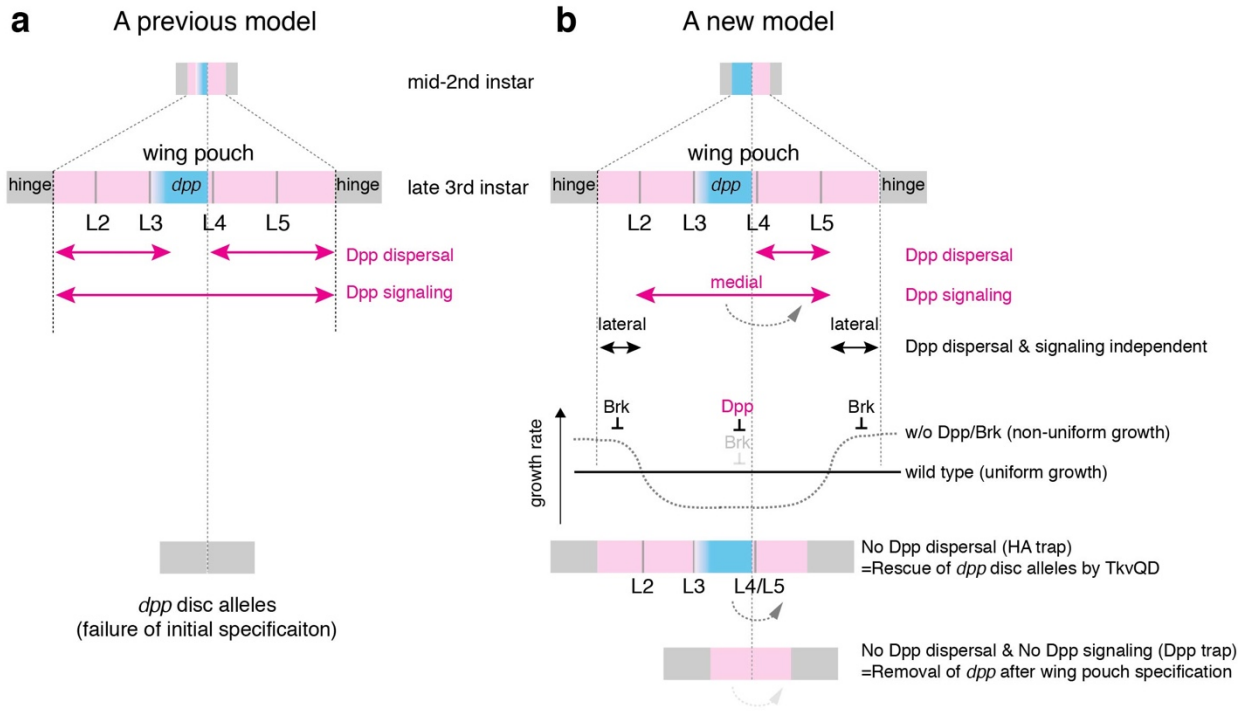

Figure 8. Distinct roles of Dpp dispersal and signaling for wing patterning and growth
a, Previous studies are based on the assumption that Dpp dispersal from the anterior stripe of cells controls patterning and growth of the entire wing pouch as implicated by complete lack of wing pouch by *dpp* disc alleles. All the growth models trying to explain the uniform growth were built on the assumption. **b**, The present study challenges the assumption and reveals distinct roles of Dpp dispersal and signaling. While critical for the posterior patterning and medial growth, Dpp dispersal is largely dispensable for anterior patterning and growth. In contrast, cell-autonomous Dpp signaling in the anterior source cells is required and sufficient for anterior patterning and growth as well as for posterior growth (though permissively). Anterior patterning and growth without Dpp dispersal requires cell-autonomous Dpp signaling through a memory of earlier signaling by initial uniform *dpp* expression. Contrast with the severe *dpp* disc alleles, neither Dpp dispersal nor signaling is critical for the lateral growth since the wing pouch specification. These results challenge the Dpp dispersal-based patterning and growth mechanisms, and lead us to propose a refined growth equalization model, in which Dpp controls medial wing pouch growth by removing a growth repressor Brk, and Brk repress the lateral wing pouch growth with higher proliferative nature to equalize growth rates. Unlike previously thought, both the Dpp signaling-dependent medial region and -independent lateral region exist within the wing pouch.

Extended Data Fig. 1

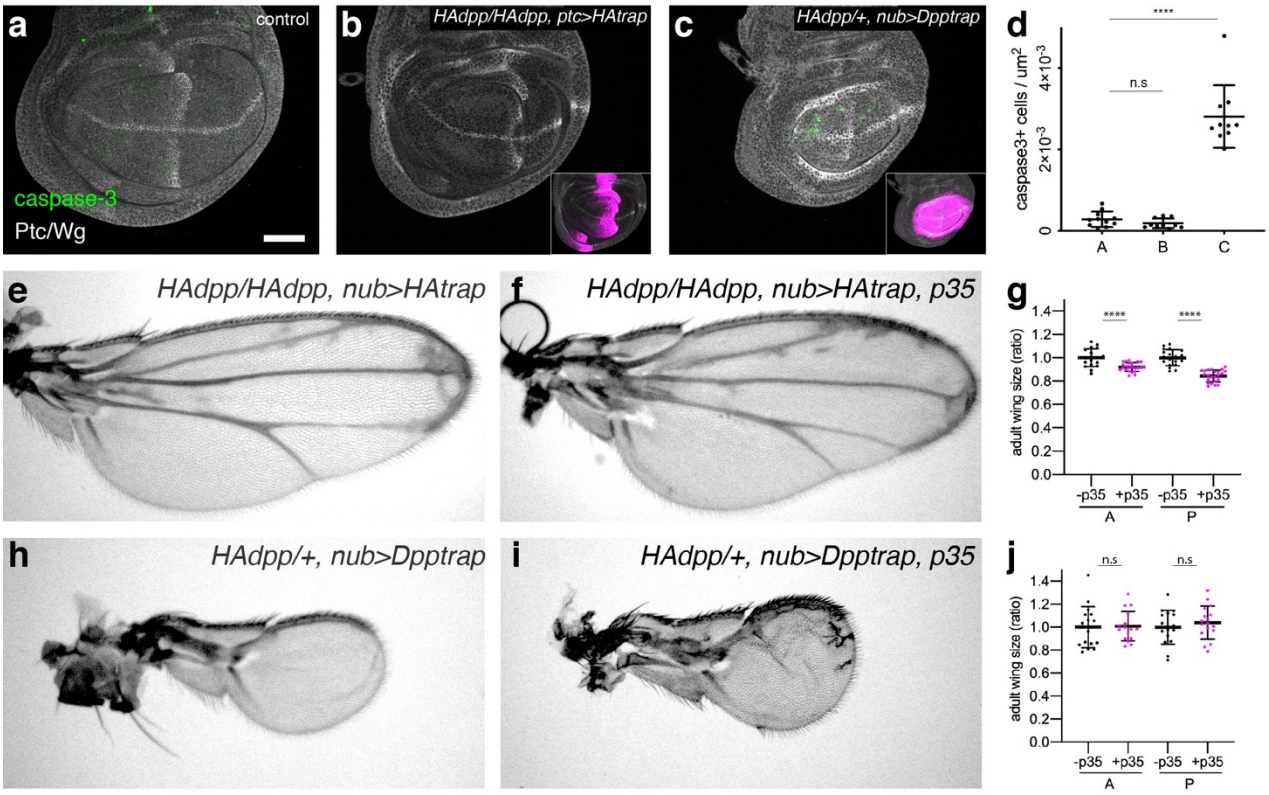

Extended Data Fig 1. Blocking cell death does not rescue growth defects caused by HA trap or Dpp trap

a-d, α-Caspase-3 and α-Ptc/Wg expression of control wing disc (**a**), *HA-dpp/HA-dpp, ptc>HA trap* disc (**b**), and *HA-dpp/+, nub>Dpp trap disc* (**c**). The insets show HA trap (mCherry) expression. Scale bar 50 μm. (**d**) Quantification of the number of α-Caspase-3 positive cells in (**a-c**). **e-g**, Adult wing of *HA-dpp/HA-dpp, nub>HAtrap* (control) (**e**) and *HA-dpp/HA-dpp, nub>HAtrap, p35* (**f**). **g**, Quantification of compartment size of (**e**, **f**). **h-j**, Adult wing of *HA-Dpp/+, nub>Dpptrap* (control) (**h**) and *HA-dpp/+, nub>Dpptrap, p35* (**i**). **j**, Quantification of compartment size of (**h**, **i**).

Extended Data Fig. 2

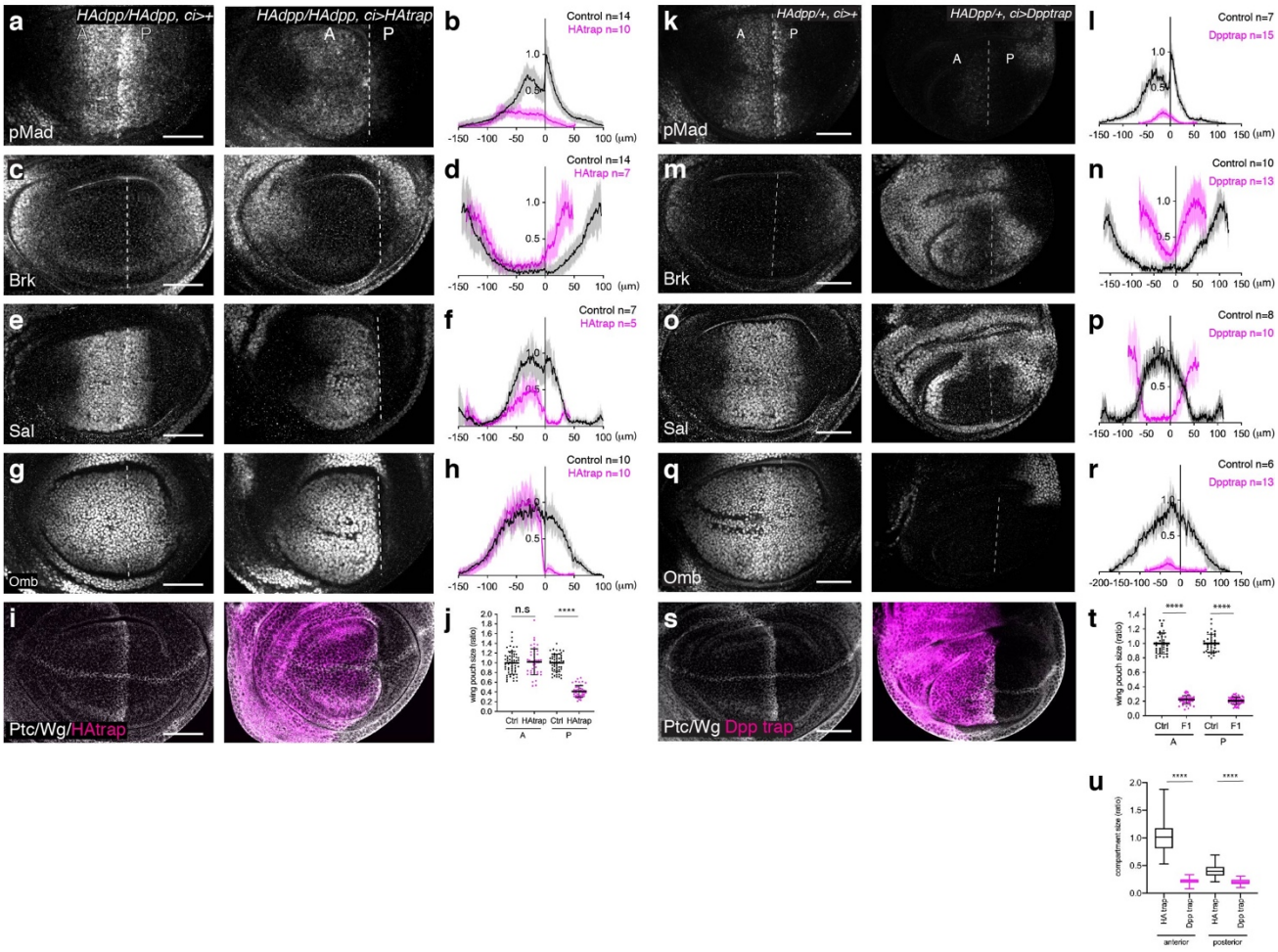

Extended Data Fig 2. Patterning and growth defects by HA trap and Dpp trap expression using *ci-Gal4*

a–**j**, Patterning and growth defects by HA trap. (**a**, **c**, **e**, **g**, **i**) α-pMad (**a**), α-Brk (**c**), α-Sal (**e**), α-Omb (**g**), α-Ptc/Wg staining and HA trap (mCherry) (**i**) of control *HA-dpp/HA-dpp, ci>+* (left) and *HA-dpp/HA-dpp, ci>HA* trap (right). (**b**, **d**, **f**, **h**) Quantification of (**a**, **c**, **e**, **g**), respectively. (**j**) Quantification of compartment size of wing pouch expressing HA trap using *ci-Gal4*. **k**-**t**, Patterning and growth defects by Dpp trap. (**k**, **m**, **o**, **q**, **s**) α-pMad (**k**), α-Brk (**m**), α-Sal (**o**), α-Omb (**q**), α-Ptc/Wg staining and HA trap (mCherry) (**s**) of control *HA-dpp/+, ci>+* (left) and *HA-dpp/+, ci>Dpp* trap (right). (**l**, **n**, **p**, **r**, **t**) Quantification of (**k**, **m**, **o**, **q**, **s**) respectively. **t**, Quantification of compartment size of wing pouch expressing Dpp trap using *ci-Gal4*. **u**, Comparison of compartment size of wing pouch upon HA trap and Dpp trap expression using *ci-Gal4* (comparison of Extended Data Fig. 1j and Extended Data Fig. 1t). Dashed white lines mark the A-P compartment border. Scale bar 50 μm.

Extended Data Fig. 3

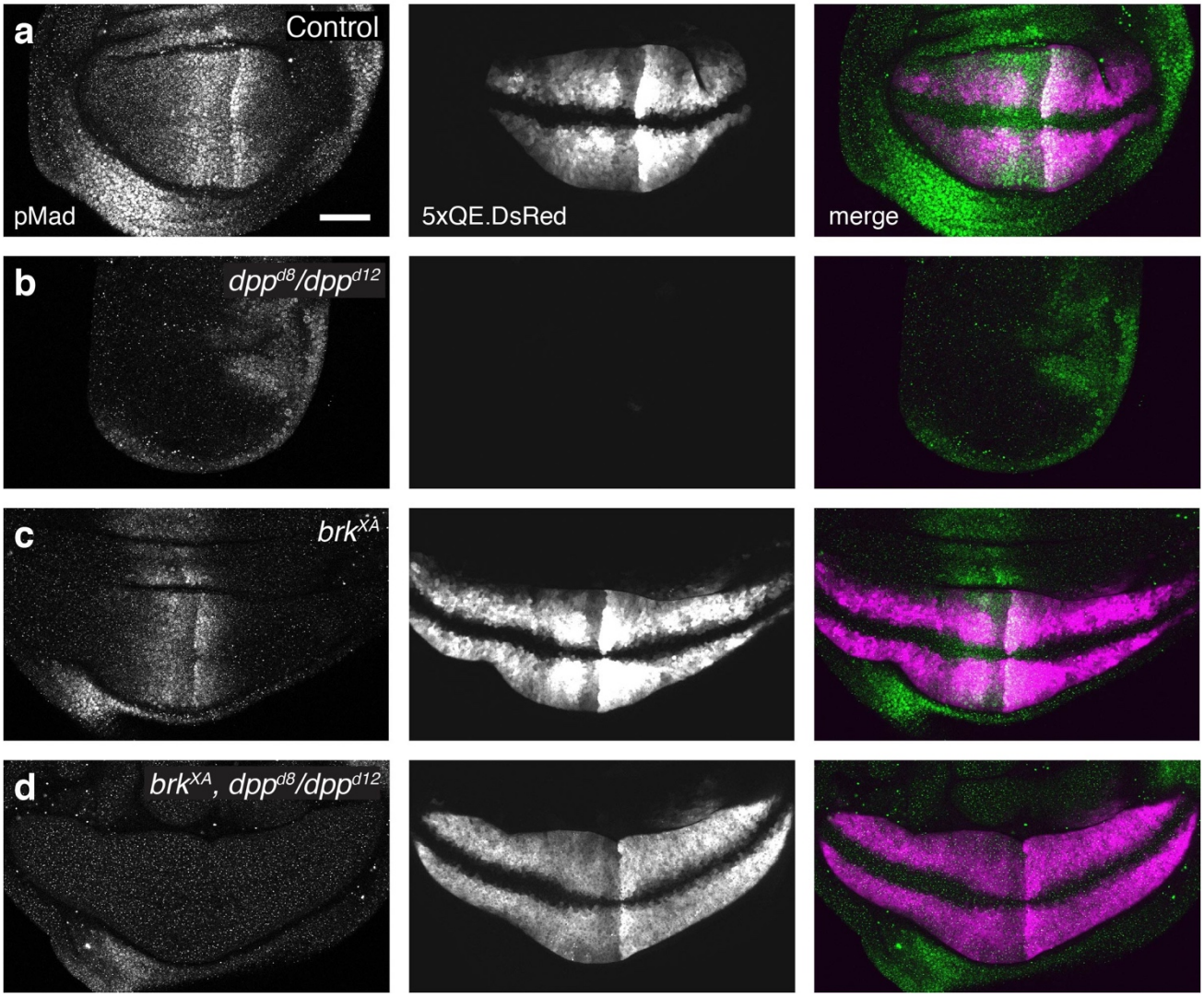

Extended Data Fig. 3 *5xQE.DsRed* reporter expression is Dpp signaling independent
a-d, α-pMad, 5xQE.DsRed, and merge of control (**a**), dpp^{d8}/dpp^{d12} (**b**), brk^{XA} (**c**), and brk^{XA}; dpp^{d8}/dpp^{d12} (**d**) wing discs. Scale bar 50 μm.

Extended Data Fig. 4

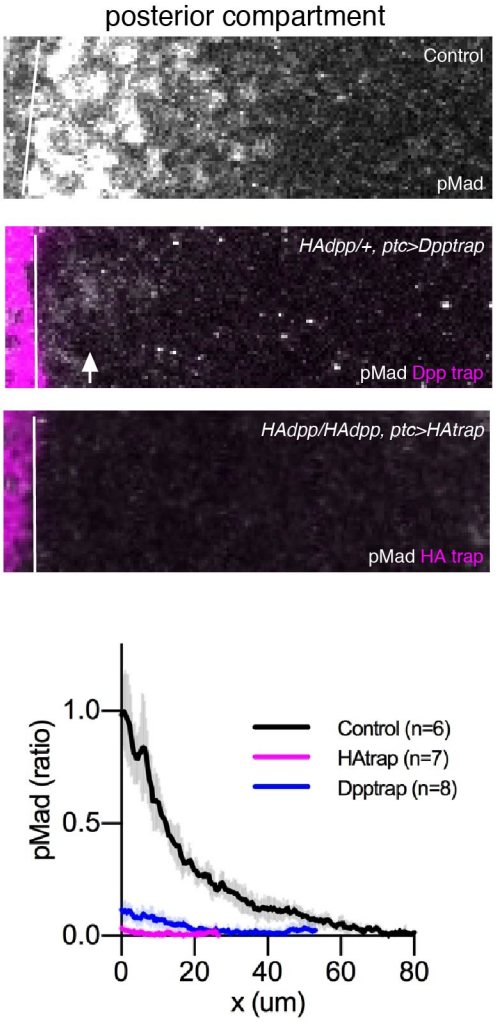

Extended Data Fig. 4 HA trap can trap Dpp more efficiently than Dpp trap

α-pMad, Dpp trap or HA trap (mCherry) in the P compartment of control wing disc (top), wing disc expressing Dpp trap using *ptc-Gal4* (middle), wing disc expressing Dpp trap using *ptc-Gal4* (bottom) wing disc. Quantification of pMad signal. Arrow indicates pMad signal by leaked Dpp from Dpp trap.

Extended Data Fig. 5

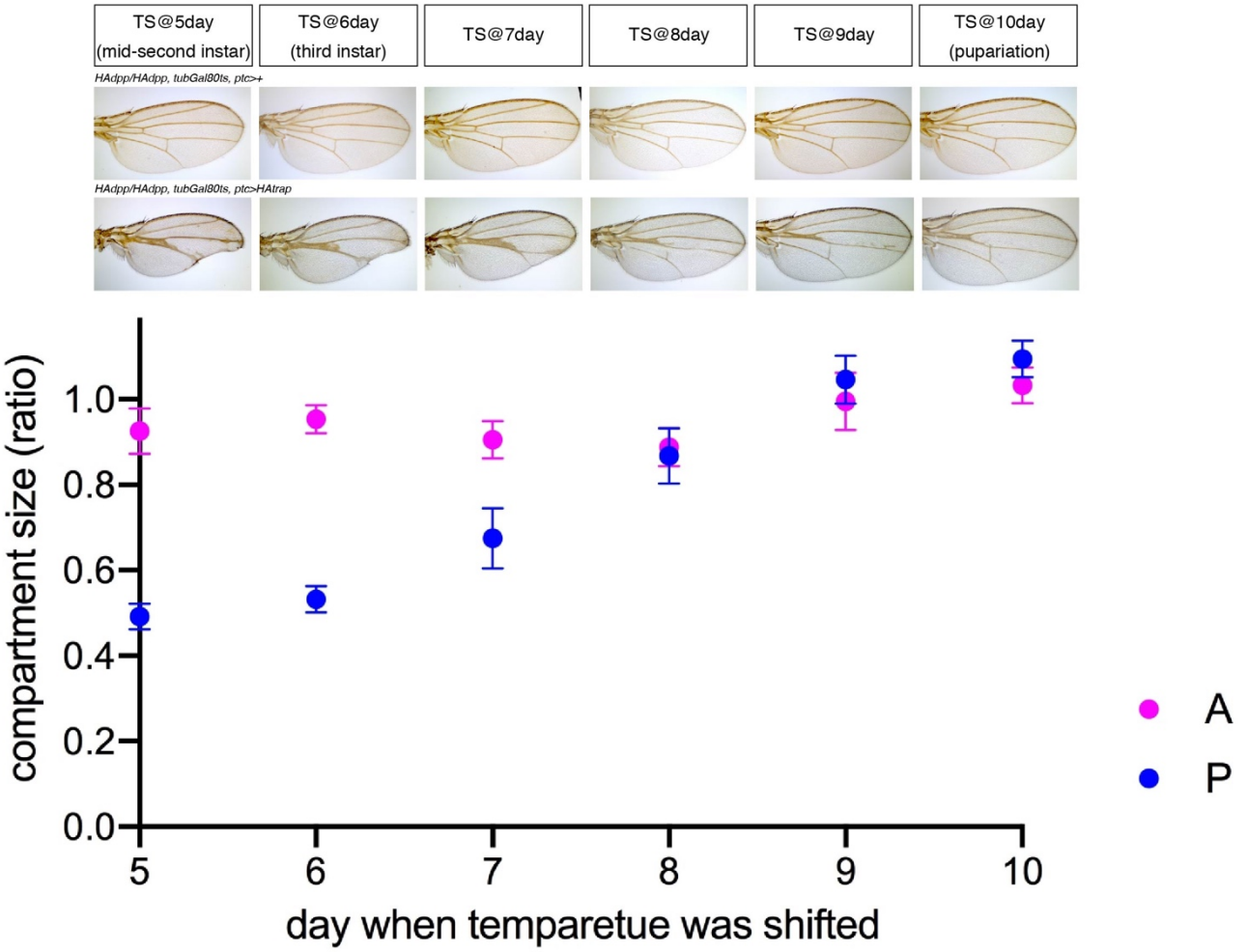

Extended Data Fig. 5 Relatively normal anterior patterning and growth by blocking Dpp dispersal at different time points

Control adult wings and adult wings expressing HA trap using *ptc-Gal4* at different time points. Crosses were shifted from 18℃ to 29℃ at indicated time point. A and P compartment size normalized against each control compartment size were plotted.

Extended Data Fig. 6

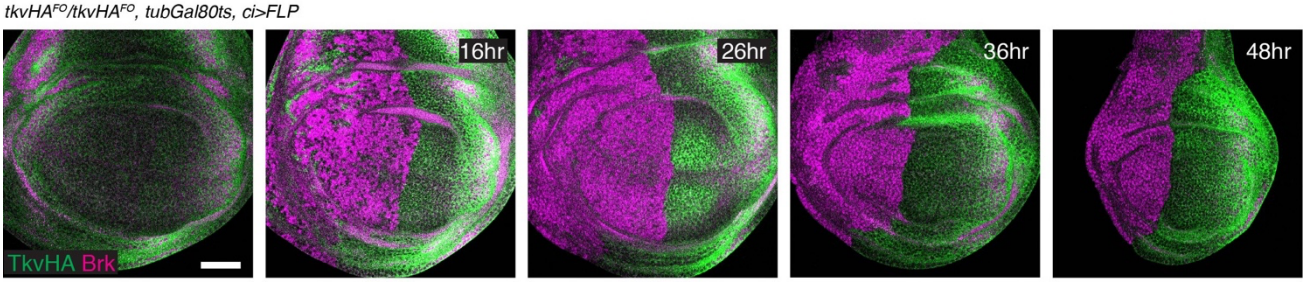

Extended Data Fig. 6 Immediate de-repression of Brk by genetic removal of *tkv*

α-HA (TkvHA^{FO}) and α-Brk staining of wing discs in which *tkv* was genetically removed from A compartment from different time points. Time shown in each figure indicates the time of dissection after temperature shift. Scale bar 50 μm.

877

Extended Data Fig. 7

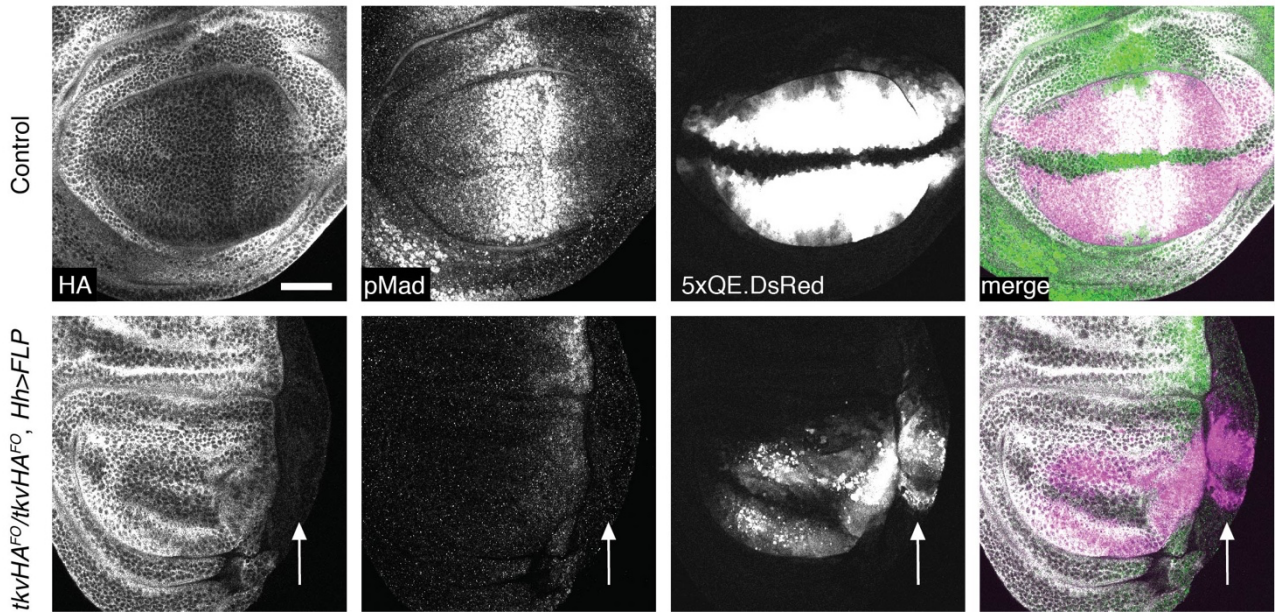

878
879

880 **Extended Data Fig. 7 A part of posterior wing pouch can grow even after removal of posterior**
881 ***tkv* from the embryonic stage**

882 α-HA (TkvHA^{FO}), α-pMad, 5xQE.DsRed, and merge of control wing disc and wing disc removing
883 *tkv* from the entire P compartment from the embryonic stage. Upon removal of *tkv* from the P
884 compartment, the 5xQE.DsRed reporter remained expressed (arrow) despite complete loss of pMad
885 signal and severe growth defects in the P compartment. Note that anterior pMad signal was also
886 affected probably because Hh target *dpp* expression is affected by the reduced number of Hh producing
887 posterior cells.

888
889